Contrib Mineral Petrol (1988) 100:107–128

Contributions to Mineralogy and Petrology

Origin of metaluminous and alkaline volcanic rocks of the Latir volcanic field, northern Rio Grande rift, New Mexico

Clark M. Johnson* and Peter W. Lipman
US Geological Survey Menlo Park, CA 94025, USA
US Geological Survey Denver, CO 80225, USA

Abstract. Volcanic rocks of the Latir volcanic field evolved in an open system by crystal fractionation, magma mixing, and crustal assimilation. Early high-SiO_2 rhyolites (28.5 Ma) fractionated from intermediate composition-magmas that did not reach the surface. Most precaldera lavas have intermediate-compositions, from olivine basaltic-andesite (53% SiO_2) to quartz latite (67% SiO_2). The precaldera intermediate-composition lavas have anomalously high Ni and MgO contents and reversely zoned hornblende and augite phenocrysts, indicating mixing between primitive basalts and fractionated magmas. Isotopic data indicate that all of the intermediate-composition rocks studied contain large crustal components, although xenocrysts are found only in one unit. Inception of alkaline magmatism (alkalic dacite to high-SiO_2 peralkaline rhyolite) correlates with initiation of regional extension approximately 26 Ma ago. The Questa caldera formed 26.5 Ma ago upon eruption of the >500 km^3 high-SiO_2 peralkaline Amalia Tuff. Phenocryst compositions preserved in the cogenetic peralkaline granite suggest that the Amalia Tuff magma initially formed from a trace element-enriched, high-alkali metaluminous magma; isotopic data suggest that the parental magmas contain a large crustal component. Degassing of water- and halogen-rich alkali basalts may have provided sufficient volatile transport of alkalis and other elements into the overlying silicic magma chamber to drive the Amalia Tuff magma to peralkaline compositions. Trace element variations within the Amalia Tuff itself may be explained solely by 75% crystal fractionation of the observed phenocrysts. Crystal settling, however, is inconsistent with mineralogical variations in the tuff, and crystallization is thought to have occurred at a level below that tapped by the eruption. Spatially associated Miocene (15–11 Ma) lavas did not assimilate large amounts of crust or mix with primitive basaltic magmas. Both mixing and crustal assimilation processes appear to require development of relatively large magma chambers in the crust that are sustained by large basalt fluxes from the mantle. The lack of extensive crustal contamination and mixing in the Miocene lavas may be related to a decreased basalt flux or initiation of block-faulting that prevented pooling of basaltic magma in the crust.

* *Present address:* Department of Geology and Geophysics, University of Wisconsin, Madison, WI 53706, USA

Offprint requests to: C.M. Johnson

Introduction

Large structural and topographic relief in the Sangre de Cristo Mountains of northern New Mexico exposes an exceptional cross section through the late-Oligocene to early-Miocene Latir volcanic field and cogenetic plutonic rocks. The Latir field can be broadly considered as part of a composite middle-Tertiary volcanic field exposed in the southern Rocky Mountains, which includes the San Juan volcanic field (Fig. 1, Steven 1975). In contrast to the nearby San Juan field, the Latir system was relatively short lived, geographically isolated, and contains regionally distinctive lithologies (Lipman 1983). These features have allowed close correlations to be made between petrologic and structural relations.

Regional extension in northern New Mexico and southern Colorado began at approximately 26 Ma, as marked by regional uplift, north-west-trending normal faults, and basaltic volcanism that was approximately coincident with the modern Rio Grande rift (Kelley and Duncan 1986; Hagstrum and Lipman 1986; Lipman and Mehnert 1975). The Latir volcanic field was the most compositionally diverse magmatic center that was active during initiation of rifting in the northern Rio Grande rift.

This paper concerns the petrology and geochemistry of the precaldera and caldera-related rocks of the Latir field exposed in the Sangre de Cristo Mountains of northern New Mexico (Fig. 2, Table 1). In addition, spatially related Miocene basalt and andesite lavas are discussed. Mineral and whole-rock chemical data indicate that both mixing and fractionation processes are responsible for the compositional diversity of the Latir rocks. Pre-extension intermediate-composition lavas mixed with primitive basalts and also assimilated significant amounts of crustal materials. In contrast, younger lavas erupted during block-faulting extension did not undergo extensive mixing and assimilation.

Geologic setting

The Latir volcanic field may be divided into four groups: 1) 28.5 to 27 Ma precaldera metaluminous basaltic-andesite to rhyolite lavas, ash-flow tuffs and hypabyssal intrusions, 2) 27–26.5 Ma alkalic dacite, comendite, and caldera-related peralkaline rhyolite lavas and a regional ash-flow tuff (Amalia Tuff), 3) 26.5–22 Ma postcaldera peralkaline granite and metaluminous granite to granodiorite plutons, and 4) 26–22 Ma alkali dacite to rhyolite and metaluminous andesite to rhyolite lavas (Lipman et al. 1986; Thompson

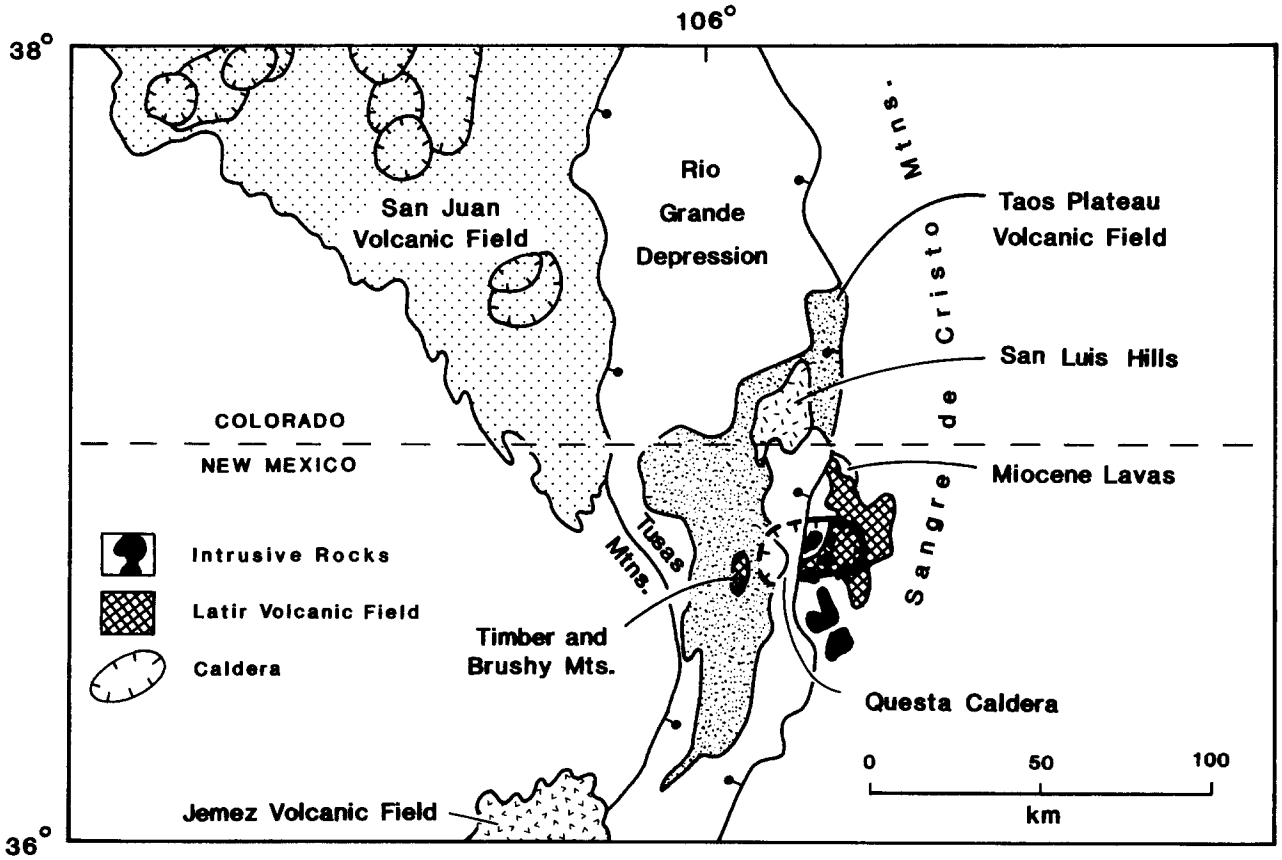

Fig. 1. Index map of northern New Mexico and southern Colorado in the Rio Grande rift region showing major Tertiary volcanic centers. Adapted from Lipman (1983)

et al. 1986). The first three groups are exposed in the Sangre de Cristo Mountains on the eastern side of the Rio Grande rift. The postcaldera peralkaline granite represents the non-erupted portion of the Amalia Tuff magma that solidified immediately following caldera formation (Johnson et al. submitted). The last group is exposed in the Timber and Brushy Mountains on a horst block in the center of the rift and consists of lavas which overlie basal Amalia Tuff (Figs. 1 and 2). Some volcanic rocks in the Tusas Mountains on the west side of the Rio Grande rift (Fig. 1; Butler 1971; Manley 1981) are distal erosional remnants of the Latir field (Lipman 1983), demonstrating that the Latir field covered an area far greater than the 1200 km^2 contiguous exposures in the Sangre de Cristo Mountains.

The precaldera and caldera-related volcanic rocks and several of the postcaldera resurgent plutons are steeply tilted, whereas the postcaldera horst lavas are not tilted (Hagstrum and Lipman 1986; Thompson et al. 1986). Late phases of the resurgent plutons within the Questa caldera are not tilted, indicating that structural disruption was restricted to the east margin of the current Rio Grande rift and occurred immediately after caldera formation at 26.5 Ma.

Early geologic mapping of the Latir field included work by McKinlay (1956, 1957) and Clark and Read (1972). Lipman and Reed (1988) and Lipman (1988) summarize recent geologic investigations of the Latir field. Other recent studies include the geochemistry and petrology of postcaldera plutons (Dillet and Czamanske 1987; Johnson et al. submitted; Czamanske and Dillet 1988) and postcaldera lavas exposed in the Timber and Brushy Mountains (Thompson et al. 1986), isotope geochemistry of the volcanic and plutonic rocks (Johnson and Lipman submitted), and paleomagnetic relations of the extrusive and intrusive rocks (Hagstrum and Lipman 1986).

Rock classifications reported in this paper are based on chemical compositions of the dominant rock types. Unit names used here for precaldera Latir rocks (Fig. 2, Table 1) are based on chemical compositions and phenocryst assemblages, and closely follow those used by Lipman and Reed (1988). We have defined rocks as metaluminous or peralkaline based on both chemical compositions and phenocryst assemblages. The metalumnous Latir rocks may also be described as calc-alkaline.

Analytical techniques

Phenocryst compositions were determined by electron-microprobe using a 9-spectrometer instrument and the Bence-Albee method of background calculation (Tables 2–5). A 15 kv accelerating voltage was used with a 15-nA specimen beam current for feldspars and a 20-nA current for all other minerals. Sr data were corrected for Si interference and checked against several homogeneous plagioclase separates analyzed by XRF; results agreed to within the estimated error of the microprobe analyses at the 2000 ppm level, which is $+/-10\%$ (1-sigma S.D.).

Major elements were analyzed using wave length-dispersive XRF at the U.S.G.S., Denver. Ferrous Fe was determined by titration. Trace element analyses (except the REEs) were made by high energy wave length-dispersive XRF (in duplicate) in the laboratory of Dr. B. Chappell at the Australian National University. Mass-absorption coefficients were measured directly for some elements and were calculated from major element compositions for others. Rb, Sr, Ba, Zr, and Nb are precise to 2–3%; Ni, Cr, and Th to 3–6%; and V, Cu, Zn, U, and Pb to 10–15% (1-sigma S.D.) for the range of concentrations reported here.

Most REE contents were determined by isotope-dilution mass-spectrometry (IDMS) at the U.S.G.S., Menlo Park as part of a companion Nd isotope study (Johnson and Lipman submitted). Several samples were analyzed by IDMS in the laboratory of Dr. G. Hanson at SUNY, Stony Brook, some of which were duplicated

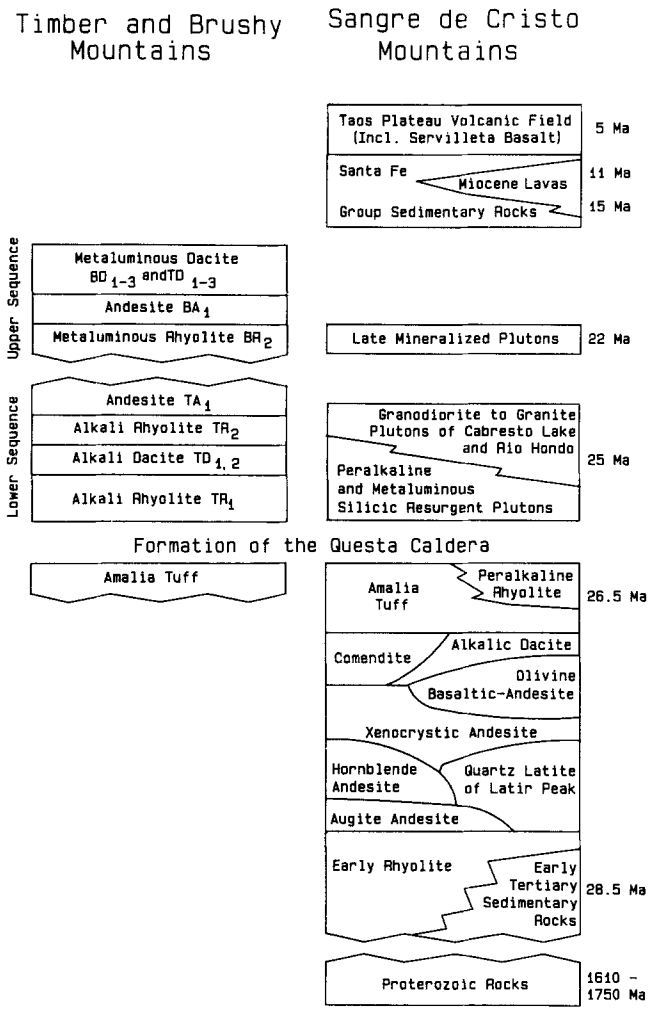

Fig. 2. Stratigraphy of Tertiary igneous rocks exposed in the Sangre de Cristo Mountains (east-rift) and Timber and Brushy Mountains (central-rift) of northern New Mexico. This paper discusses the precaldera and caldera-related Latir rocks and spatially-associated Miocene lavas exposed in the Sangre de Cristo Mountains. Unit names of postcaldera Latir lavas exposed in the Timber and Brushy Mountains from Thompson et al. (1986). Postcaldera Latir plutonic rocks exposed in the Sangre de Cristo Mountains are discussed in Johnson et al. (submitted). Ages and Tertiary stratigraphy of the Sangre de Cristo Mountains from Reed et al. (1983), Lipman et al. (1986), and Lipman and Reed (1988). Early rhyolite unit includes Tuff of Tetilla Peak from Lipman and Reed (1988)

at Menlo Park. Precision is better than 1% (1-sigma S.D.) for 1 ppm of Ce, Nd, Sm, Eu, Gd, Dy, Er, and Yb. Several samples were also analyzed by INAA at the U.S.G.S., Reston, and the values are similar to those obtained on similar samples analyzed by IDMS, though significantly less precise.

Phenocryst mineralogy and chemistry

Precaldera metaluminous rocks

Feldspar. Feldspars are present in all of the metaluminous rocks, although no fresh feldspar was found in the olivine basaltic-andesite. Plagioclase core compositions vary greatly; rim compositions are relatively homogeneous within samples (Table 2, Fig. 3). Plagioclase compositional trends within the early rhyolite, hornblende andesite, and quartz latite are smooth (Figs. 3A, 3C, 3E), suggesting that these hydrous magmas did not undergo dramatic changes in water pressures and/or temperature during crystallization. Compositional trends of plagioclase in the augite andesite have slight bends (Fig. 3B), however, suggesting that water contents may have increased during late crystallization in these relatively dry magmas (e.g. Brown and Parsons 1981).

The xenocrystic andesite contain up to 15% xenocrystic alkali and plagioclase feldspar and quartz. Feldspar xenocrysts can be as large as 3 cm, and are pink, strongly resorbed and fractured, but generally optically homogeneous. Primary plagioclase is distinguished by euhedral and subhedral morphologies and well-developed twinning and zoning. Plagioclase cores in a relatively uncontaminated sample (123) have similar compositions as those of other Latir rocks with similar whole-rock compositions, but rims are anomalously K-rich and probably reflect late-stage contamination with a K-rich crustal component (Fig. 3D). All primary plagioclases in one strongly contaminated sample (118) are altered, and only xenocrystic feldspar compositions for this sample are plotted in Fig. 3D. All feldspar xenocrysts are heterogeneous within grains and are anomalously K-rich in comparison to primary plagioclase from the least-contaminated sample (123). The disequilibrium textures and unusual compositions of the xenocrystic feldspars suggests that they were not derived by mixing with silicic magmas, but may instead reflect partial dissolution of annealed anti-perthitic feldspars derived from Proterozoic basement rocks. The presence of large (up to 1 cm) quartz xenocrysts also indicates derivation from silicic basement rocks.

Strontium and anorthite contents of plagioclase are well-correlated in most cases, and the ternary diagrams in Fig. 3 are contoured for Sr contents. Approximate equilibrium Sr concentrations for plagioclase phenocrysts may be estimated using *whole-rock* Sr concentrations and reasonable mineral/melt distributions coefficients (K_D). Inasmuch as plagioclase is the dominant phenocryst in most of the Latir rocks, the groundmass Sr contents will be less than those of the whole-rocks, resulting in an overestimation of calculated equilibrium plagioclase Sr concentrations using *whole-rock* Sr concentrations. This overestimation will be small, however, since phenocryst contents are generally less than 15%. K_Ds of 2 and 5 were assumed for intermediate and silicic-composition rocks, respectively (Mahood and Hildreth 1983; Nash and Crecraft 1985; Arth 1976; Henderson 1982), and the calculated equilibrium plagioclase values are marked in Fig. 3.

The high Sr contents of plagioclase phenocrysts in the early rhyolite strongly suggest that cores of many plagioclase crystals are out of equilibrium with the host rhyolite, and were derived from high-Sr intermediate-composition parental magmas. Plagioclase phenocrysts from the augite andesite, quartz latite, and xenocrystic andesite have Sr contents which are consistent with crystallization from their host magmas. Plagioclase phenocrysts from a relatively silicic quartz latite sample (139) have Sr contents similar to those of the mafic samples, suggesting that most of the plagioclase phenocrysts were derived from a more mafic parental magma that was similar to the majority of quartz latite samples. Plagioclase rims in one hornblende andesite (79L-73) have anomalously high Sr contents (Fig. 3C), indicating that late-stage mixing with a high-Sr magma occurred. The anomalously high Sr contents of all plagioclase

Table 1. Mineralogy of precaldera and caldera-related Latir rocks

Unit	Major phenocrysts	Minor Phenocrysts	Accessory minerals
Peralkaline granite	Sanidine > Quartz	Arfvedsonite > Tetrasilicic Mica > Acmite	Sphene > Zircon > > Apatite
Peralkaline rhyolite	Sanidine > Quartz	Arfvedsonite > Tetrasilicic Mica > Fe-Ti Oxides	Rare zircon
Late-erupted Amalia Tuff	Sanidine > Quartz	Arfvedsonite > Tetrasilicic Mica > Fe-Ti Oxides	Sphene > Zircon > > Apatite
Early-erupted Amalia Tuff	Quartz > Sanidine	Tetrasilicic Mica > Acmite > Fayalite > Ferrohedenbergite > Fe-Ti Oxides	Sphene > Apatite > Zircon > > Allanite
Comendite	Sanidine	Fe-Ti Oxides	Trace zircon
Alkalic dacite	Aphyric		
Olivine basaltic-andesite	Olivine + Plagioclase > Augite	Fe-Ti Oxides	
Xenocrystic andesite	Plagioclase > Hornblende > Hypersthene > Augite > Biotite Up to 15% xenocrysts of Alkali and Plagioclase Feldspar + Quartz	Fe-Ti Oxides	Trace Apatite
Latir Peak Quartz Latite	Plagioclase > > Hornblende > Biotite	Quartz > Biotite > Fe-Ti Oxides	Sphene > Apatite > Zircon
Latir hornblende andesite	Hornblende > > Augite > Plagioclase > Orthopyroxene	Fe-Ti Oxides	
Augite andesite	Plagioclase + Augite	+/− Olivine + Fe-Ti Oxides	Apatite
Early rhyolite	Plagioclase > Quartz > Biotite > Sanidine	Fe-Ti Oxides +/− Hornblende	Sphene > Apatite > Zircon

in hornblende andesite 110 (Fig. 3C) may indicate derivation from a high-Sr parental magma.

Pyroxene. Augite is common in the augite andesite, hornblende andesite, and xenocrystic andesite, and is rare in the quartz latite. Many augite phenocrysts in the Latir rocks are reversely zoned with high-Mg rims (Table 3, Fig. 4). Augite in the xenocrystic andesite (123 and 118) and one augite andesite (119), however, are normally zoned. Augites in all of the Latir rocks have high proportions of non-quadrilateral components, usually tschermakite + acmite, up to 12%.

MgO and Cr_2O_3 contents of augite are well-correlated, varying from 13.5 to 18 and <0.02 to 0.85%, respectively, and Cr_2O_3 contents are contoured in Fig. 4. High MgO and Cr_2O_3 rims suggest that many of the intermediate-composition Latir magmas were mixed with relatively primitive magmas during the late stages of crystallization. Although the high-Mg rims might be explained by extensive crystallization (>10%) of Fe-Ti oxides, or progressive oxidation of the magma due to H_2 loss (Czamanske et al. 1981), the high Cr_2O_3 rims cannot be explained by such mechanisms. The low-MgO and -Cr_2O_3 rims in the xenocrystic andesite may reflect continued crystallization.

Hypersthene is present only in the hornblende andesite and xenocrystic andesite. Hypersthene compositions are relatively restricted in the Latir rocks and no significant zoning was found. Hypersthene compositions appear to be approximately in equilibrium with coexisting clinopyroxene.

Biotite. Biotite phenocrysts occur in the early rhyolite, quartz latite, hornblende andesite and xenocrystic andesite. Compositions vary most in the early rhyolite, from $Ph_{42}An_{35}Sd_{24}$ to $Ph_{60}An_{26}Sd_{14}$ (Table 4). Samples containing biotite as the only hydrous phenocryst have octahedral Mg/(Mg+Fe) ratios of 0.44 to 0.55, whereas samples which also contain hornblende have ratios of 0.63 to 0.67. Biotite compositions in the hornblende andesite and quartz latite average $Ph_{58}An_{23}Sd_{19}$ with octahedral Mg/(Mg+Fe) ratios varying from 0.58 to 0.67. Biotite compositions of the xenocrystic andesite are more magnesian, averaging $Ph_{69}An_{22}Sd_{09}$, with octahedral Mg/(Mg+Fe) ratios of 0.73 to 0.77.

Hornblende. All amphiboles in the metaluminous Latir rocks are calcic hornblende. Edenitic hornblende (tetrahedral Al = 1.0) with a restricted range in Mg/(Mg+Fe) ratios occurs as small euhedral phenocrysts in some samples of the early rhyolite (Table 5). Hornblendes in the precaldera andesite and quartz latite have tetrahedral Al between 1.0 (edenite) and 2.0 (hastingsite), with a small pargasite component. The higher tetrahedral Al contents of hornblendes in the intermediate-composition rocks, as compared to those in the early rhyolite, are consistent with their inferred higher liquidus temperatures (Helz, 1973, 1976; Gilbert et al. 1982). Mg/(Mg+Fe) ratios vary widely in hornblendes in the quartz latite and hornblende andesite; Mg/(Mg+Fe) ratios generally increase toward the rims. These variations are similar to those observed in most augite phe-

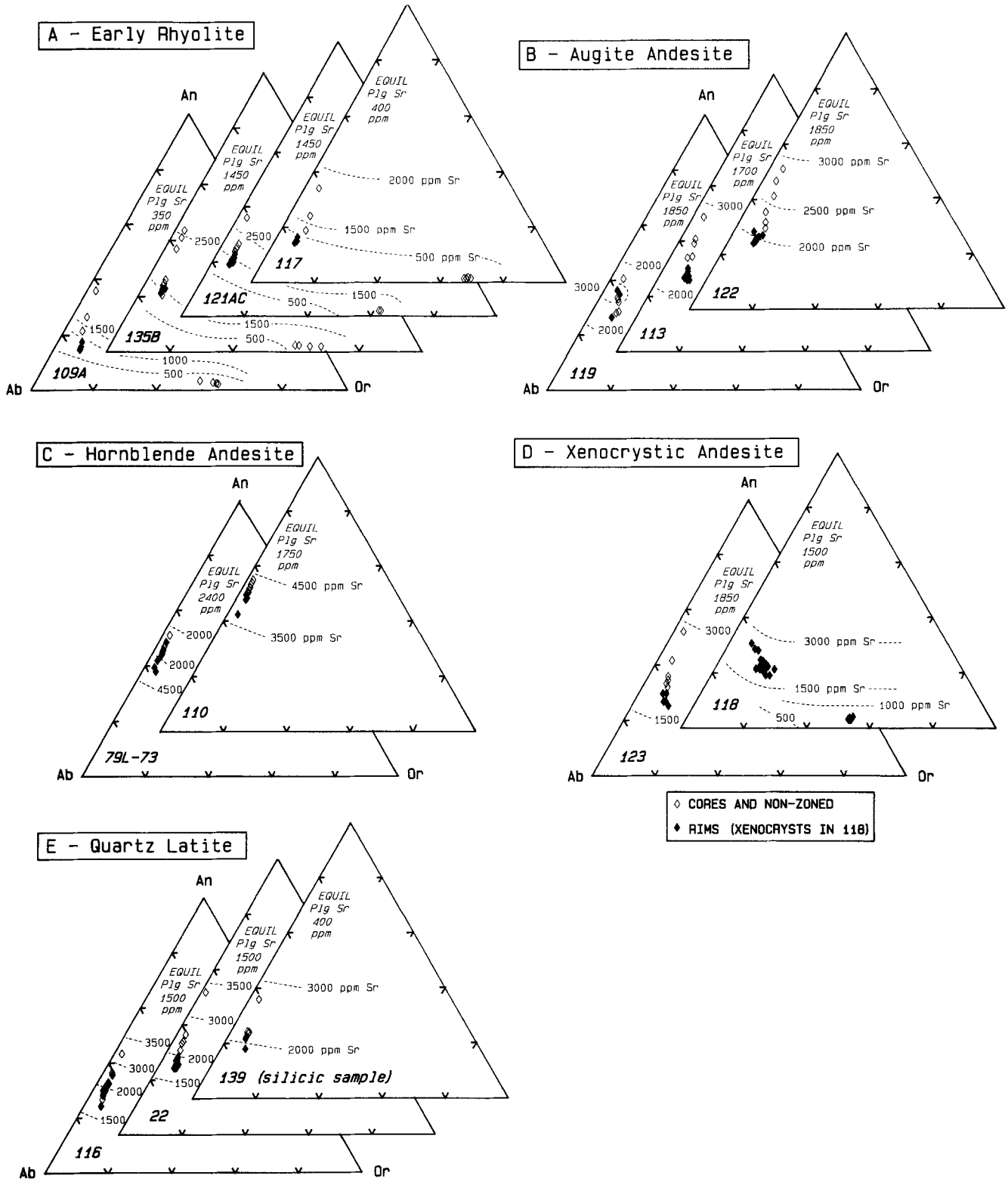

Fig. 3A–E. Feldspar compositions for representative precaldera metaluminous Latir rocks showing Sr concentrations in ppm. Greater than 95% of the analyses fall within the contours. Calculated "equilibrium" Sr concentrations are given for plagioclase, based on *whole-rock* Sr contents and bulk K_Ds = 5 and 2 for rhyolite and intermediate-composition rocks, respectively. Note that only xenocryst compositions for xenocrystic andesite 118 are plotted

nocrysts, and may indicate mixing with relatively Mg-rich magmas. Hornblendes in the xenocrystic andesites have restricted Mg/(Mg+Fe) ratios and high tetrahedral Al contents of 1.7 to 2.1.

Hornblende in the hornblende andesite occurs as 1) large euhedral phenocrysts, 2) glomerocrysts with clinopyroxene and lesser amounts of orthopyroxene, and 3) rims around large anhedral orthopyroxene phenocrysts. There

Table 2. Representative analyses of feldspars from the Latir volcanic field

	Early rhyolite			Latir Peak Quartz Latite				Augite andesite		Latir hornblende andesite
	109A-3 core	109A-3A middle	109A-3B rim	116-1 rim	116-11 core	139-2 non-zoned	139-4 core	122-1 core	122-5B rim	110-10 non-zoned
SiO_2	59.08	63.09	65.52	59.46	56.62	61.69	58.59	57.66	61.63	55.23
Al_2O_3	25.29	22.13	19.02	24.84	27.50	23.13	25.56	26.94	24.04	27.01
FeO	0.22	0.20	0.16	0.17	0.18	0.19	0.19	0.27	0.40	0.50
MgO	0.02	0.01	0.01	0.01	0.02	0.00	0.01	0.05	0.03	0.08
CaO	7.44	3.60	0.27	6.18	9.01	5.14	7.45	8.66	5.43	10.63
SrO	0.203	0.058	0.018	0.295	0.338	0.190	0.362	0.351	0.277	0.536
Na_2O	7.36	9.61	5.15	8.80	6.12	8.74	7.19	5.39	6.87	5.82
K_2O	0.49	1.34	10.09	0.70	0.41	0.94	0.54	0.79	1.17	0.39
Total	100.10	100.04	100.24	99.74	100.20	100.02	99.89	100.11	99.85	100.20
X_{An}	0.356	0.172	0.013	0.295	0.433	0.244	0.359	0.412	0.257	0.516
X_{Ab}	0.616	0.752	0.404	0.665	0.543	0.703	0.610	0.543	0.677	0.462
X_{Or}	0.028	0.076	0.583	0.040	0.024	0.053	0.031	0.045	0.066	0.022
$D_{Sr\text{-}wr}$	32.3	9.3	2.8	3.3	3.8	8.0	15.1	3.2	2.5	5.1

Table 2 (continued)

Xenocrystic andesite		Comendite			Amalia Tuff				Peralkaline rhyolite
118A-3 xenocryst	118B-3 xenocryst	140A-1 non-zoned	140A-2 rim	140A-2A core	205-1 non-zoned	40-3 core	40-3A rim	27-2 non-zoned	124-1 non-zoned
65.17	63.08	65.63	64.25	65.77	66.28	66.49	67.06	66.06	66.95
19.03	22.19	19.37	21.82	19.36	19.09	19.06	19.58	19.26	18.33
0.12	0.17	0.15	0.23	0.16	0.12	0.10	0.19	0.13	0.44
0.02	0.01	0.02	0.01	0.02	0.01	0.01	0.01	0.01	0.01
0.49	4.23	0.97	3.11	1.24	0.23	0.26	0.27	0.25	0.01
0.103	0.182	<0.010	<0.010	<0.010	<0.010	<0.010	<0.010	<0.010	<0.010
5.67	7.25	6.04	7.23	6.34	5.64	5.53	6.17	5.74	7.13
9.19	2.90	7.80	3.27	6.79	8.83	8.51	6.62	8.69	6.92
99.79	100.01	99.98	99.92	99.68	100.20	99.95	99.90	100.14	99.79
0.024	0.202	0.047	0.147	0.060	0.011	0.013	0.013	0.012	0.000
0.451	0.633	0.506	0.669	0.552	0.484	0.501	0.613	0.490	0.605
0.525	0.165	0.447	0.184	0.388	0.505	0.486	0.374	0.498	0.395
1.2	2.1	–	–	–	–	–	–	–	–

$D_{Sr\text{-}wr}$ is feldspar/whole-rock distribution coefficient for Sr
X_{An} = mole fraction of $CaAl_2Si_2O_8$, X_{Ab} = mole fraction of $NaAlSi_3O_8$, X_{Or} = mole fraction of $KAlSi_3O_8$

is no correlation of Mg/(Mg+Fe) ratios with the nature of hornblende occurrence, although euhedral phenocrysts tend to have the highest tetrahedral Al contents. Hornblende glomerocrysts or rims on orthopyroxene have the lowest tetrahedral Al contents, suggesting lower temperatures of equilibration.

Accessory minerals. Sphene, zircon and apatite are present in the early rhyolite and quartz latite. Sphene can be up to 2 mm long in the quartz latite, and is the dominant accessory mineral in the precaldera metaluminous rocks. Apatite is common in the augite andesite, and occurs in trace amounts in the xenocrystic andesite.

Precaldera and caldera-related alkalic rocks

Phenocryst mineralogy and compositions of the alkalic rocks are distinct from those of the metaluminous rocks. Sanidine is the only feldspar in phyric samples. Mafic silicates include alkali amphibole and pyroxene, and Al-poor brown mica (tetrasilicic mica). Biotite is found in lithic-rich whole-rock samples of the Amalia Tuff, but is absent from vitrophyres and cogenetic lavas, and is interpreted as xenocrystic. Determination of the mineralogy of the Amalia Tuff is hindered by the rarity of pumice, and relies on analyses of basal vitrophyres, cogenetic lavas, and cogenetic peralkaline granite.

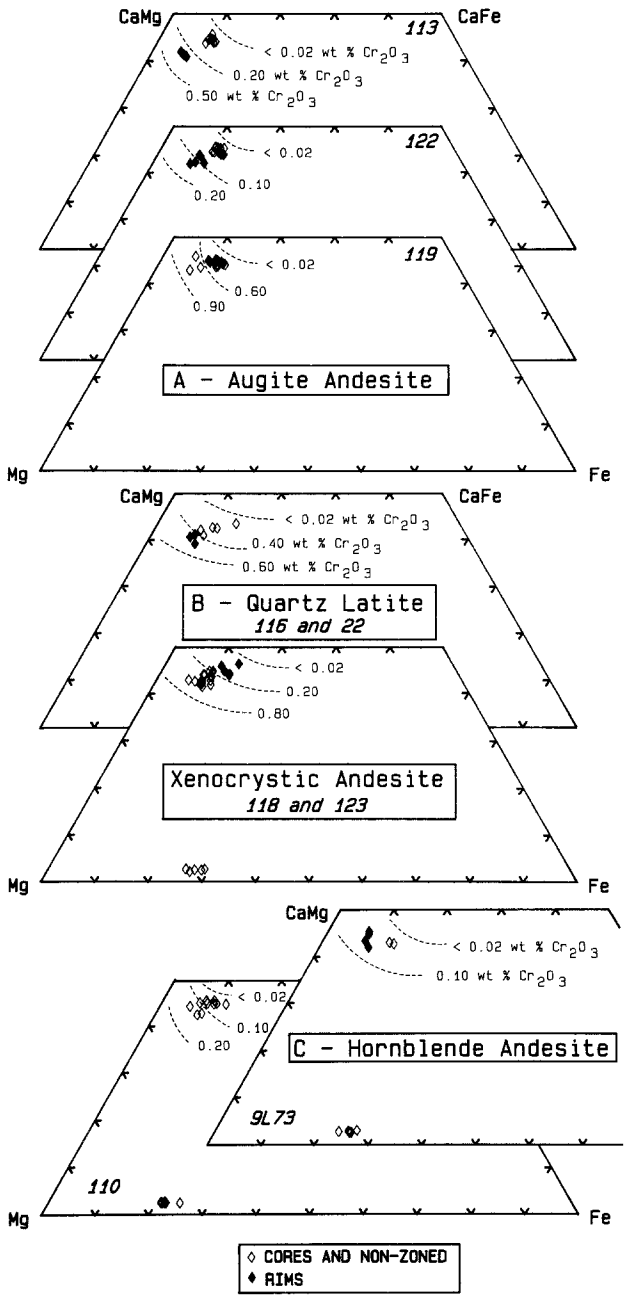

Fig. 4. Pyroxene compositions for representative intermediate-composition precaldera Latir rocks showing Cr_2O_3 concentrations in wt %. Greater than 95% of the analyses fall within the contours

Sanidine. Sanidine is present in the comendite, Amalia Tuff, and peralkaline rhyolite. The comendite contains euhedral to subhedral sodic sanidine to anorthoclase phenocrysts ranging from $An_{06}Ab_{55}Or_{39}$ to $An_{15}Ab_{67}Or_{18}$ (Fig. 5A). Euhedral sodic sanidine occurs throughout the Amalia Tuff, ranging from $An_{01}Ab_{47}Or_{52}$ to $An_{01}Ab_{61}Or_{38}$ (Fig. 5B). Core compositions become slightly more sodic upward in the tuff, and all samples except the basal tuff contain sanidine phenocrysts that are zoned to sodic compositions toward the rims. Densely welded tuff which has been severely K-metasomatized contains sanidine with compositions that are similar (Ab_{50} to Ab_{58}) to those in the unaltered outflow sheets. Sanidine in the peralkaline rhyolite is not zoned and compositions are similar to those of sanidine rims in the upper Amalia Tuff. This is consistent with geologic relations which indicate that the peralkaline rhyolite was erupted during the waning stages of caldera collapse (Lipman 1983). Sanidine/quartz ratios vary systematically through the Amalia Tuff from <1 in the basal tuff to >1 in the late-erupted portions of the tuff and peralkaline rhyolite, to approximately 2 in the peralkaline granite (Dillet and Czamanske 1987).

Mafic silicates. All mafic silicates in the comendite are altered, but pseudomorphs of olivine (presumably fayalite) and amphibole are present. It is not clear if pyroxene was a phenocryst in the comendite. A distinctive anhedral brown mica similar to that in the peralkaline rhyolite and cogenetic granite (Czamanske and Dillet 1988) is preserved in some sanidine phenocrysts in the comendite.

Early-erupted portions of the Amalia Tuff contain very few mafic minerals, but some samples contain a distinctive anhedral brown mica that is similar in appearance to tetrasilicic mica analyzed in the peralkaline rhyolite and cogenetic granite (below). Euhedral biotite is found in some lithic-rich whole-rock samples, but this mica is interpreted as xenocrystic. Acmite, fayalite, ferrohedenbergite, and brown mica are present in basal vitrophyres north of the caldera.

Tetrasilcic mica was analyzed in the peralkaline rhyolite (Table 4) and cogenetic peralkaline granite (Czamanske and Dillet 1988). Endmember tetrasilicic mica has only Si (4 cations) in the tetrahedral site (Seifert and Schreyer 1965), but the term is appropriately applied to any mica with greater than 3 Si cations in the tetrahedral site. Tetrahedral Si varies from 3.30 to 3.65 cations in the Latir tetrasilicic micas. The only other reported natural occurrence of tetrasilicic mica is in the Charlennes comendite in the Mont-Dore massif, France (Robert and Maury 1979). The presence of tetrasilicic mica is diagnostic of silicic peralkaline rocks.

Arfvedsonitic amphibole is present in late-erupted portions of the Amalia Tuff and peralkaline rhyolite (Table 5). Arfvedsonite exists as individual phenocrysts, as well as rims on relatively Fe- and Ca-rich amphibole cores in the peralkaline granite (Czamanske and Dillet 1988). Arfvedsonite is in equilibrium with tetrasilicic mica in all samples. Czamanske and Dillet (1988) note, however, that tetrasilicic mica replaces biotite and katophoritic to richteritic amphibole cores in some samples of peralkaline granite. These relations have not been observed in any extrusive samples, but this may be due to the rarity of suitable samples of pumice and phyric lavas.

Accessory minerals. Zircon is present in the comendite, Amalia Tuff and peralkaline rhyolite. Semi-quantitative mineral separates of early- and late-erupted portions of the Amalia Tuff indicate that the early tuff contains approximately 5% quartz and sanidine phenocrysts and approximately 0.02% total accessory minerals: approximately 0.01% sphene, 0.005% apatite, 0.001% zircon, and $<<0.001\%$ allanite. The late tuff contains approximately 20% quartz and sanidine phenocrysts and approximately 0.1% total accessory minerals. Sphene/apatite and zircon/apatite ratios increase and allanite is absent. The mineralogy of the cogenetic peralkaline granite continues the trends defined by the eruptive sequence of the Amalia Tuff; the granite contains 30–50% phenocrysts, sphene and zircon abundances increase relative to apatite, and allanite is ab-

Table 3. Representative analyses of pyroxenes from the Latir volcanic field

	Xenocrystic andesite					Augite andesite	
	4-C3 non-zoned	118-C3 non-zoned	123-O1 non-zoned	123-C1A core	123-C1B rim	119-C3 non-zoned	122-C15 core
SiO_2	52.59	51.20	53.67	51.80	52.36	52.42	52.18
TiO_2	0.41	0.82	0.21	0.48	0.38	0.31	0.28
Al_2O_3	2.36	3.01	0.97	2.40	1.51	1.52	1.78
Cr_2O_3	0.29	0.02	0.11	0.20	0.12	0.02	0.09
Fe_2O_3	1.67	2.79	1.10	2.82	2.47	2.52	2.93
FeO	5.21	5.99	16.55	4.94	5.78	6.72	5.91
MnO	0.17	0.23	0.53	0.21	0.30	0.39	0.28
MgO	16.72	15.44	25.50	16.05	15.54	14.90	14.83
CaO	19.81	20.15	1.36	20.71	21.01	20.88	20.90
Na_2O	0.58	0.52	0.04	0.45	0.49	0.55	0.70
Total	99.81	100.17	100.04	100.06	99.96	100.23	99.88
Si^{IV}	1.931	1.891	1.957	1.909	1.938	1.943	1.936
Al^{IV}	0.069	0.109	0.042	0.091	0.062	0.057	0.064
Al^{VI}	0.033	0.023	0.000	0.013	0.004	0.009	0.014
Fe^{+2}	0.160	0.185	0.505	0.152	0.179	0.208	0.183
Fe^{+3}	0.046	0.077	0.030	0.078	0.069	0.070	0.082
Mg	0.915	0.850	1.386	0.882	0.857	0.823	0.820
Ca	0.779	0.797	0.053	0.818	0.833	0.831	0.831
Na	0.041	0.037	0.003	0.032	0.035	0.040	0.050
Mn	0.005	0.007	0.016	0.007	0.009	0.012	0.009
Ti	0.011	0.023	0.006	0.013	0.011	0.009	0.008
Cr	0.009	0.001	0.003	0.006	0.004	0.000	0.003
% Quad	90.11	87.67	95.83	88.99	91.34	91.15	89.36
X_{Wo}	42.03	43.51	2.73	44.17	44.56	44.58	45.29
X_{En}	49.34	46.40	71.30	47.62	45.87	44.23	44.71
X_{Fs}	8.63	10.09	25.97	8.21	9.57	11.19	10.00

sent (Czamanske and Dillet 1988; Johnson et al. submitted).

Whole-rock chemistry

Precaldera metaluminous rocks

Major element compositions of basaltic-andesite to rhyolite Latir rocks (Table 6) are similar to those of other Tertiary volcanic rocks in the southern Rocky Mountains (Lipman et al. 1978). Precaldera and postcaldera Latir rocks span similar compositional ranges, from 53 to 78% SiO_2.

Early rhyolite. Lithic-poor whole-rock samples of Tetilla Peak Tuff and associated lavas range from 75 to 77% SiO_2 (Fig. 6). Both glassy and devitrified samples have lost Na_2O and gained K_2O. The relatively low Sr contents (<200 ppm, Fig. 7A) for many samples suggest extensive feldspar fractionation (e.g. Mahood and Hildreth 1983; Nash and Crecraft 1985). Th, HREE contents, and Nb/Zr ratios, vary widely, indicating varied amounts of accessory mineral fractionation (Figs. 7 and 8). The rocks do not have a strong apparent Eu anomaly, although this may be obscured moderate by depletion in the MREEs.

Basaltic-andesite to dacite lavas. These lavas include the augite andesite (62–64% SiO_2), hornblende andesite (58–66% SiO_2), xenocrystic andesite (62–65% SiO_2), and olivine basaltic-andesite (53–62% SiO_2). The major element compositional trends, REE patterns, Th-SiO_2 variations and Nd/Zr ratios of these units are similar, in contrast to their varied phenocryst assemblages (Figs. 6–8), suggesting derivation from chemically similar parental magmas. Nb/Zr ratios and HREE contents of the precaldera Latir rocks are lower than those of the intermediate-composition postcaldera Latir rocks (Figs. 7 and 8).

Quartz latite. The most voluminous precaldera unit is the Latir Peak Quartz Latite (Lipman and Reed 1988). The quartz latite is preserved as lavas and hypabyssal intrusions, the majority of which have relatively homogeneous compositions of 65–67% SiO_2. The silicic margin of one intrusion contains 73% SiO_2 (139), and this is the only sample found to fall in an apparent compositional gap between the intermediate-composition units and the early rhyolite. Both glassy and devitrified samples have variable K_2O and Na_2O contents due to post-eruption alteration. Although TiO_2 and CaO contents continue the trends with SiO_2 of the andesites, the quartz latite is distinguished by relatively high MgO contents (Fig. 6).

Precaldera alkalic rocks

The alkalic dacite (64–66% SiO_2) and comendite (70–72% SiO_2) are lower in MgO and Sr contents than metaluminous Latir rocks of similar SiO_2 content, and markedly higher

Table 3 (continued)

Augite andesite	Latir hornblende andesite					Latir Peak Quartz Latite	
122-C15A rim	110-O2 non-zoned	110-C4 non-zoned	9L73-C1 core	9L73-C1A rim	9L73-O1 non-zoned	116-C2 core	116-C2A rim
52.00	53.98	52.63	50.06	52.55	53.41	50.72	53.46
0.50	0.20	0.24	0.84	0.54	0.18	0.07	0.57
2.02	1.52	1.43	4.14	2.26	1.57	4.91	2.22
0.03	0.02	0.02	0.03	0.09	0.04	0.71	0.46
2.16	2.02	1.86	3.32	2.03	1.56	2.32	0.88
5.86	13.74	7.23	7.20	5.66	15.55	8.34	4.36
0.23	0.42	0.41	0.28	0.16	1.18	19.53	19.58
16.46	27.59	14.68	14.18	16.75	26.01	13.56	18.08
19.96	1.20	20.93	19.04	19.84	0.34	0.27	0.16
0.35	0.02	0.54	0.75	0.48	0.20	0.56	0.22
99.57	100.71	99.97	99.84	100.36	100.04	100.99	99.99
1.924	1.933	1.955	1.866	1.924	1.941	1.873	1.943
0.076	0.064	0.045	0.134	0.076	0.059	0.131	0.062
0.012	0.000	0.018	0.048	0.022	0.007	0.078	0.044
0.181	0.411	0.225	0.224	0.173	0.465	0.261	0.133
0.060	0.055	0.052	0.093	0.056	0.037	0.064	0.019
0.908	1.473	0.813	0.787	0.914	1.402	0.753	0.983
0.791	0.046	0.833	0.760	0.778	0.052	0.772	0.756
0.025	0.001	0.039	0.054	0.034	0.001	0.046	0.025
0.007	0.013	0.013	0.009	0.005	0.007	0.006	0.005
0.014	0.005	0.007	0.024	0.015	0.008	0.019	0.006
0.001	0.001	0.001	0.001	0.002	0.012	0.001	0.022
91.28	93.57	92.28	83.50	90.49	93.71	83.56	91.73
42.09	2.39	44.54	42.90	41.72	2.53	43.36	40.57
48.27	76.30	43.45	44.44	48.99	72.92	42.17	52.15
9.65	21.31	12.01	12.66	9.29	24.56	14.38	7.13

Fe_2O_3 by charge balance (Lindsley 1983). X_{Wo} = mole fraction $CaSiO_3$, X_{En} = mole fraction $MgSiO_3$, X_{Fs} = mole fraction $FeSiO_3$

in REE and most trace element contents, particularly Zr and the HREEs (Figs. 9 and 10, Table 6). The alkalic dacite and comendite are strongly oxidized. Alkali mobility is also a problem in the comendite samples, and this has resulted in low calculated agpaitic indexes of 0.90–0.95. The comendite is clearly peralkaline, however, since quartz is absent in these silicic rocks and the rocks have high Y, Zr, and Nb contents (e.g. Macdonald and Bailey 1973; Watson 1979).

Amalia Tuff and peralkaline rhyolite

The Amalia Tuff is relatively homogeneous in major element compositions, although slight variations (e.g. 1% SiO_2) would not be recognized due to alteration or variable lithic contents in whole-rock samples. Glassy pumices contain up to 8 wt% volatiles, and the largest variations in MgO, Na_2O, K_2O, and CaO contents are in the most hydrated samples (not listed in Table 6). One outflow section on the eastern margin of the Rio Grande rift north of the caldera (Cedro Canyon) contains devitrified tuffs that contain up to 7% K_2O. This K-metasomatism is restricted to the groundmass, however, as sanidine compositions in these samples are similar to those in fresh tuff (Fig. 5B). An approximate average Amalia Tuff major element composition, estimated from lithic-poor bulk-tuff and relatively non-hydrated glassy pumice is 75 to 77% SiO_2, 4.5% Na_2O, 4.5 to 4.8% K_2O, <0.5% CaO and MgO, and 1.6 to 1.9% FeO_{total}. This composition is similar to that of devitrified samples of the peralkaline rhyolite lavas and fresh samples of peralkaline granite.

Stratigraphic and mineralogical correlations of outflow sections permit reconstruction of the trace element concentrations that existed in the Amalia Tuff magma chamber prior to eruption. Concentrations vary systematically with stratigraphic height for most trace elements (Fig. 11), but some trends are obscured due to reliance on bulk-tuff samples. Pumice is present throughout the Amalia Tuff, although most fragments cannot be sampled because of dense welding and rheomorphism. Nonwelded tuff in the northeast portion of the Latir field (#1 Camp Creek) includes valley fills that probably represent the earliest phases of the eruption. Arfvedsonite-bearing densely welded tuff caps this section, indicating that late-erupted outflow tuff is also preserved at this locality. Most pumices from the #1 Camp Creek section are relatively homogeneous in trace element composition, although the highest pumice sampled just below inception of welding (41P) has distinctly lower Rb, Y, Nb, HREEs and higher Zr, LREES, and Eu in comparison to stratigraphically lower pumices (e.g. 204P; Figs. 11 and 12). These trends are consistent with those observed in the vitrophyres, western outflow sections, and peralkaline rhyolite lavas that are considered to represent progressively later stages of eruption based on mineralogy and geologic

Table 4. Representative analyses of micas from the Latir volcanic field

	Early rhyolite					Latir Peak Quartz Latite			Xenocrystic andesite		Peralkaline rhyolite
	135-1	121AC-7	117-6	109A-6	109A-12B	139-4	116-18	22-8	125-3	123-1	124-5B
SiO_2	36.26	36.67	36.18	38.28	36.54	37.06	37.34	36.67	36.90	38.68	39.92
TiO_2	4.67	4.42	3.98	3.77	4.52	4.34	4.48	3.67	4.17	5.14	2.43
Al_2O_3	13.59	15.25	13.64	12.70	14.00	13.58	14.25	14.72	14.54	13.25	6.31
FeO	20.35	16.16	21.73	14.41	15.41	16.56	15.14	16.88	15.82	10.70	28.47
MnO	0.29	0.34	0.55	0.50	0.55	0.24	0.17	0.18	0.20	0.07	4.38
MgO	11.35	12.95	10.43	16.22	14.60	14.21	14.90	14.19	14.56	18.06	3.28
CaO	0.02	0.04	0.06	0.01	0.02	0.03	0.07	0.06	0.01	0.03	0.01
Na_2O	0.44	0.45	0.41	0.51	0.52	0.41	0.49	0.37	0.49	0.67	0.56
K_2O	9.01	9.31	9.05	9.40	9.00	9.28	8.94	9.21	9.16	9.20	9.04
H_2O^+	3.92	3.99	3.90	4.03	3.98	3.99	4.03	4.00	4.01	4.12	3.63
Total	99.90	99.57	99.92	99.82	99.14	99.69	99.81	99.94	99.86	99.92	98.03
Si^{IV}	2.771	2.754	2.786	2.848	2.753	2.788	2.777	2.751	2.757	2.818	3.293
Al^{IV}	1.229	1.246	1.214	1.152	1.247	1.212	1.223	1.249	1.243	1.182	0.708
Al^{VI}	0.000	0.104	0.024	0.000	0.000	0.000	0.026	0.053	0.038	0.000	0.002
Ti	0.268	0.250	0.230	0.211	0.256	0.245	0.251	0.207	0.234	0.282	0.154
Fe^{+2}	1.300	1.015	1.399	0.897	0.971	1.042	0.942	1.060	0.989	0.652	1.963
Mn	0.019	0.022	0.036	0.031	0.035	0.015	0.011	0.012	0.013	0.004	0.308
Mg	1.292	1.450	1.197	1.799	1.640	1.593	1.652	1.587	1.622	1.962	0.403
Sum Oct	2.875	2.840	2.885	2.900	2.898	2.887	2.882	2.919	2.895	2.855	2.733
Ca	0.002	0.003	0.005	0.001	0.001	0.003	0.006	0.005	0.001	0.002	0.001
Na	0.065	0.065	0.061	0.073	0.076	0.060	0.070	0.053	0.071	0.095	0.069
K	0.878	0.892	0.889	0.893	0.865	0.891	0.848	0.882	0.873	0.855	0.954
Sum A	0.945	0.960	0.955	0.967	0.942	0.954	0.924	0.940	0.945	0.952	1.019
X_{Ph}	0.45	0.51	0.41	0.62	0.57	0.55	0.57	0.54	0.56	0.69	0.15
X_{An}	0.32	0.22	0.33	0.28	0.24	0.27	0.24	0.22	0.23	0.22	0.85
X_{Sd}	0.23	0.27	0.25	0.10	0.20	0.18	0.19	0.23	0.21	0.09	0.00

All Fe calculated as FeO. H_2O^+ calculated assuming full hydroxyl site. Structural formula calculated using 22 oxygens. X_{Ph} = mole fraction $KMg_3(AlSi_3)O_{10}(OH)_2$, X_{An} = mole fraction $KFe_3(AlSi_3)O_{10}(OH)_2$, X_{Sd} = mole fraction $K(Fe_2Al)(Si_2Al_2)O_{10}(OH)_2$

relations. Trace element contents of intracaldera Amalia Tuff are similar to those of samples from the upper #1 Camp Creek section and the western outflow sections, although interpretation is hindered by dense-welding and structural repetitions within the caldera.

Miocene lavas

Miocene (15–11 Ma) andesite and Ne- and Hy-normative alkali olivine basalt overlie the Latir rocks in the northern part of the volcanic field. Ne-normative basalts contain 46% SiO_2 and Hy-normative basalts contain 49% SiO_2 (Fig. 6). The andesites are lower in MgO and higher in Na_2O contents as compared to precaldera Latir lavas of similar SiO_2 content. REE contents of the Miocene andesites are similar to those of precaldera Latir lavas, but contrast with those of the Miocene basalts. Nb/Zr ratios of the Miocene lavas continue an apparent increase with decreasing age for the region, from low ratios in the precaldera Latir rocks through higher ratios in the postcaldera Latir lavas (Fig. 7). The Miocene lavas are bimodal with respect to Sr contents, defining a high-Sr suite (1500 to 2100 ppm), and a low-Sr suite (500–900 ppm). An important contrast between the Miocene and Latir hornblende andesites is the significantly lower Ni contents in the Miocene lavas; the Ni contents in the Miocene lavas are close to those expected for moderately fractionated rocks, whereas the Ni contents of the precaldera andesites are anomalously high.

Discussion

Evidence for magma mixing

Mixing between intermediate to silicic-composition magmas and relatively mafic magmas is widely recognized. The presence of fine-grained mafic inclusions (Bacon and Metz 1984; Bacon 1986; Koyaguchi 1986a) provides evidence for incomplete mixing, whereas reversely zoned phenocrysts (Sakuyama 1979; 1981; Luhr and Carmichael 1980; McMillan and Dungan 1986; Shimizu and Roex 1986) and elevated compatible-element contents (Novak and Bacon 1986) indicate more complete mixing.

Magma mixing in the Latir rocks is indicated by reversely zoned augite and hornblende phenocrysts (Fig. 4, Table 5), and is additionally supported by whole-rock chemical data. Ni-SiO_2 and Ni-Th relations (Figs. 7C and 13) indicate that many of the intermediate-composition Latir rocks have Ni contents that are too high for their parental magmas to have fractionated olivine. This is supported by Cr-SiO_2 and Cr-Th variations. Moreover, because Ni is highly compatible in mafic magmas, the high Ni values cannot be explained by coupled assimilation/crystallization

Table 5. Representative analyses of amphiboles from the Latir volcanic field

	Early rhyolite	Latir Peak Quartz Latite			Latir hornblende andesite		Xenocrystic andesite		Amalia Tuff	Peralkaline rhyolite
	109A-2	22-6	116-12	116-G-F	9L73-R3	110A-R3	4-2	123-5	42A-3	124-5
SiO_2	48.86	41.43	44.39	45.97	44.97	44.80	40.59	42.33	51.51	50.29
TiO_2	1.01	1.87	1.40	1.55	1.75	2.15	4.00	2.88	0.48	0.48
Al_2O_3	5.56	11.18	9.12	8.39	8.46	9.42	12.73	11.20	2.07	0.87
Fe_2O_3	3.16	4.41	4.52	4.26	3.61	3.28	3.24	3.45	2.61	4.35
FeO	9.06	14.34	12.18	9.49	11.39	8.58	8.75	8.34	10.32	21.73
MnO	0.97	0.40	0.38	0.33	0.37	0.26	0.11	0.16	3.69	5.78
MgO	15.52	10.13	12.16	14.33	13.28	15.04	13.83	14.68	14.03	3.17
CaO	11.22	10.95	11.25	11.43	10.91	11.32	11.14	11.15	7.09	1.26
Na_2O	1.60	1.79	1.53	1.47	1.91	2.03	2.46	2.34	4.04	8.27
K_2O	0.64	1.49	1.00	0.81	0.97	0.84	1.02	1.21	0.79	0.76
Total	97.60	97.99	97.93	98.03	97.62	97.72	97.87	97.74	96.63	96.96
Si^{IV}	7.106	6.258	6.590	6.705	6.657	6.537	5.971	6.214	7.572	7.952
Al^{IV}	0.894	1.742	1.410	1.295	1.343	1.463	2.029	1.786	0.356	0.047
Al^{VI}	0.060	0.249	0.186	0.149	0.133	0.157	0.179	0.152	0.001	0.111
Fe^{+2}	1.101	1.811	1.513	1.157	1.410	1.047	1.076	1.025	0.763	2.872
Fe^{+3}	0.345	0.501	0.505	0.467	0.402	0.360	0.358	0.382	0.842	0.531
Mg	3.363	2.281	2.690	3.116	2.928	3.269	3.032	3.212	3.072	0.762
Mn	0.119	0.051	0.048	0.041	0.046	0.032	0.014	0.020	0.465	0.757
Ti	0.111	0.213	0.157	0.170	0.195	0.236	0.443	0.318	0.048	0.058
Sum Oct	5.100	5.106	5.097	5.100	5.114	5.102	5.101	5.108	5.001	5.079
Ca^{M4}	1.749	1.772	1.791	1.786	1.730	1.769	1.757	1.754	1.122	0.222
Na^{M4}	0.151	0.122	0.112	0.115	0.156	0.129	0.142	0.138	0.829	1.700
Na^{A}	0.301	0.402	0.329	0.302	0.392	0.446	0.558	0.528	0.301	0.850
K^{A}	0.118	0.286	0.190	0.151	0.183	0.156	0.191	0.226	0.154	0.151
Sum A	0.419	0.686	0.519	0.453	0.575	0.602	0.749	0.754	0.452	1.000

Fe_2O_3 calculated as midpoint of permissible values by method of Papike et al. (1974)
Structural formula calculated using 23 oxygens

or mixing/crystallization involving either basalt or rhyolite endmembers (Fig. 13).

The Ni contents of the precaldera Latir rocks may be interpreted as mixing of a dacitic magma (66–70% SiO_2) with varying amounts of high-Ni basalt (250–300 ppm). Following this model, the proportion of basaltic component would vary from less than 10% for the quartz latite and silicic hornblende andesite to as much as 40% for mafic hornblende andesite and olivine basaltic-andesite. The dominant component was probably not more silicic than dacite because 1) with the possible exception of the xenocrystic andesite, rhyolitic phenocrysts/xenocrysts are absent in the intermediate-composition Latir rocks, and 2) inclusion of small amounts of basalt into rhyolite magma results in quenched fine-grained inclusions rather than homogeneous mixed magma (Bacon 1986; Sparks and Marshall 1986); such inclusions are rare in the Latir rocks.

The relations illustrated in Figs. 7C and 13 are insensitive to several types of mixing and fractionation. Because less than 10% olivine fractionation would deplete the Ni content of basalt magma by a factor of 2, mixing between intermediate-composition magma and fractionated basalt would not be readily recognized since both would have similar Ni contents. Such mixing should still be recognizable in phenocryst chemistry, however. Post-mixing fractionation of hornblende and clinopyroxene would substantially deplete Ni contents, and therefore the measured values may represent minimum ones. The high Ni contents of the mafic hornblende andesite and olivine basaltic-andesite may reflect mixing just prior to eruption.

Thompson et al. (1986) interpreted relatively high MgO contents in postcaldera Latir lavas, as compared to MgO contents calculated for low-pressure fractionation paths using EQUIL (Nielson 1985), as indicative of mixing between primitive and relatively evolved magma. Fractionation paths calculated using EQUIL and the most primitive olivine basaltic-andesite (81L-46) in the precaldera Latir sequence also indicate that MgO contents may be anomalously high. As noted above, the intermediate-composition Miocene lavas have significantly lower MgO and Ni contents than those of Latir rocks of similar SiO_2 contents (Figs. 6, 7, and 13), suggesting that magma mixing was not important in the Miocene lavas.

Mixing involving high-Ni basalts places important constraints on the geometry and history of the magmatic center. Basalt injected into the Latir system cannot reflect plumes of less-dense magma separating from a cumulate pile (e.g. Huppert et al. 1986) because any magma separating from olivine will be Ni-depleted. Late-stage mixing involving high-Ni basalt probably is not a reflection solely of magma chamber dynamics, such as vertical movement of mafic magma within a compositionally-stratified magma chamber. Instead, such mixing must ultimately be related to the basalt flux into the crust.

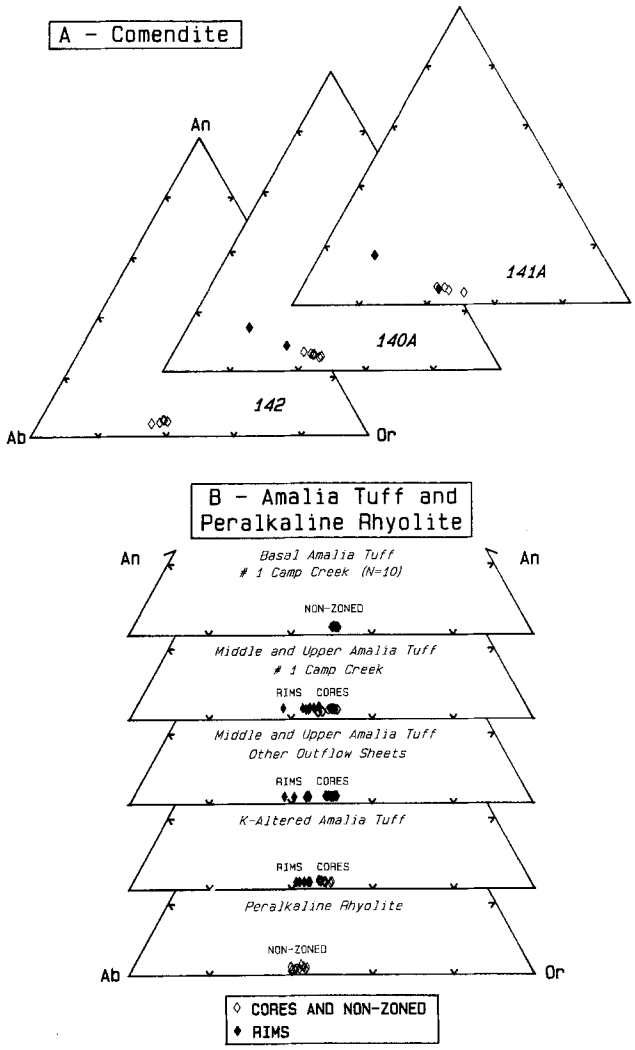

Fig. 5. Feldspar compositions for representative precaldera and caldera-related alkalic rocks

Evidence for crustal components

Isotopic data demonstrate that the majority of the Latir magmas assimilated Proterozoic crust to varying degrees, whereas Miocene lavas assimilated relatively little crust (Johnson and Lipman submitted). ϵ_{Nd} values and initial $^{87}Sr/^{86}Sr$ ratios of the precaldera rocks vary from -4 to -7 and 0.7050 to 0.7075, respectively, with the least radiogenic Nd and most radiogenic Sr restricted to the early rhyolite. $^{206}Pb/^{204}Pb$ ratios vary from 17.5 to 18.4, consistent with interaction with relatively non-radiogenic lower crust. The precaldera and caldera-related alkalic rocks have ϵ_{Nd} values of -6 to -7, initial $^{87}Sr/^{86}Sr$ ratios of 0.708 to 0.720, and relatively radiogenic $^{206}Pb/^{204}Pb$ ratios of 18.9 to 19.5, suggesting involvement of middle or upper crustal lithologies. In contrast, the Miocene lavas have initial $^{87}Sr/^{86}Sr$ ratios of 0.7039 to 0.7045 and ϵ_{Nd} values of $+1$ to -3, which may be interpreted as primary mantle values. Although $^{206}Pb/^{204}Pb$ ratios vary from 17.3 to 18.2, indicating limited involvement of relatively non-radiogenic crust, the primitive Sr and Nd isotopic compositions constrain the amount of assimilation to less than 10%.

Most trace element contents of the intermediate-composition and silicic-composition Latir rocks can be explained by reasonable amounts of crystal fractionation (<90%) of basaltic magmas with compositions similar to those of the early-rift (26 Ma) Hindsdale basalts which occur north of the Latir field (Lipman and Mehnert 1975; Thompson and Johnson 1987). The high Pb contents of most of the intermediate to silicic Latir rocks require, however, incorporation of a crustal component. If bulk-assimilation/crystallization is assumed (DePaolo 1981), the elevated Pb contents are best explained by high ratios of assimilation to crystallization (1:2) and high Pb contents for the assimilant (40 ppm), using reasonable Pb K_Ds (0.4 to 0.8; Henderson 1982). Such high Pb contents are unusual for most crustal rocks (Taylor 1964), and are not found in the Proterozoic rocks exposed in northern New Mexico (J. Reed, personal commun. 1984; Wooden and Johnson, unpublished data 1988). Assimilation (mixing) of partial melts of the crust, rather than bulk rocks, is an attractive mechanism for increasing trace element contents of the assimilant without requiring unusual crustal compositions. The same equations describing bulk-assimilation/crystallization may be applied to mixing crustal melts during crystallization.

Several studies have argued that assimilation of crustal rocks (e.g. DePaolo and Johnson 1979; Grove and Baker 1984) or mixing basaltic and silicic magmas (e.g. Eichelberger 1978; Koyaguchi 1986b) will retard the Fe enrichment that is often considered characteristic of calc-alkaline fractionation (Miyashiro 1974). Fe enrichment in the Latir rocks occurs at higher SiO_2 contents than in the Miocene lavas (Fig. 14), consistent with the hypothesis that retardation in Fe-enrichment is accompanied by addition of a silicic component. Crystal fractionation and coupled crystallization/assimilation trends calculated using EQUIL illustrate the strong retardation of Fe-enrichment during assimilation (mixing) of a silicic component (bulk rock or melt) during crystallization (Fig. 14). Although calculations using EQUIL are better suited to more tholeiitic compositions (e.g. Dungan et al. 1986) than the parental alkali basalt used here (115), the calculations illustrate the marked shift in Fe-enrichment during addition of silicic components.

Constraints on parental magmas

Major elements. General constraints may be placed on the degree of fractionation of some units using the program XLFRAC (Stormer and Nichols 1978), although crystal fractionation using major elements is difficult to model for the Latir rocks because of the effects of mixing and assimilation documented above. Depending on the relative amounts of mixing and assimilation involved, however, these effects will tend to cancel each other out. Development of fractionation models is further hindered by the lack of preserved Fe-Ti oxides and olivine phenocrysts, and by post-eruption oxidation of Fe and alkali mobility.

Major element fractionation models calculated using XLFRAC and appropriate phenocryst assemblages suggest that the precaldera Latir rocks are related to tholeiitic or mildly alkalic (Hy-normative) basaltic parental magmas. Strongly alkalic parental magmas are not consistent with major and trace element compositions and phenocryst assemblages. The major element composition of the most mafic Latir basaltic-andesite (81L-46, 53% SiO_2) can be approximated by 45 to 50% crystallization of olivine, clinopyroxene, and plagioclase from a parental basalt similar to early-rift Hindsdale tholeiite lavas (Thompson and Johnson 1987) (sum $R^2 = 1.9$). Major element variations within

Table 6. Representative whole-rock chemical analyses of volcanic rocks from the Latir volcanic field and Miocene lavas

	Early rhyolite			Augite andesite		Latir hornblende andesite		Latir Peak Quartz Latite			
	121AC	109B	135B	113	119	110	79L-73	22	116	139	PWL
SiO_2	76.4	76.0	77.3	63.1	63.4	59.1	63.7	65.6	66.8	73.1	65.9
TiO_2	0.21	0.20	0.20	0.78	0.79	0.92	0.90	0.60	0.59	0.35	0.56
Al_2O_3	12.6	12.8	12.0	15.4	15.3	14.4	15.8	15.4	14.7	13.9	15.7
Fe_2O_3	1.29	0.88	1.23	5.26	4.33	3.22	3.70	2.46	3.14	1.97	2.45
FeO	0.16	0.19	0.20	0.52	1.19	3.69	1.70	1.98	1.53	0.27	2.04
FeO_{TOTAL}	1.33	0.98	1.31	5.29	5.12	6.63	5.03	4.22	4.38	2.04	4.27
MnO	<0.02	0.04	<0.02	0.07	0.06	0.11	0.07	0.07	0.09	<0.02	0.07
MgO	0.33	0.23	0.27	2.15	2.82	5.44	2.10	2.30	2.31	0.86	2.25
CaO	1.02	0.53	0.87	5.05	4.50	6.37	4.20	3.86	3.99	1.18	4.02
Na_2O	3.56	3.69	3.24	3.97	4.17	3.53	3.70	4.08	3.91	2.86	4.47
K_2O	4.48	5.46	4.73	3.75	3.49	3.11	3.50	3.59	3.03	5.55	2.44
P_2O_5	0.08	<0.05	0.06	0.38	0.37	0.43	0.51	0.30	0.27	0.12	0.28
LOI	0.99	0.78	1.11	2.65	2.29	1.57	0.58	0.68	0.48	2.73	3.45
AI	0.85	0.93	0.87	0.69	0.70	0.64	0.69	0.69	0.66	0.77	0.64
Ba	610	200	1180	1135	1330	1180		1240	1190	1000	1450
Rb	119	140	106	81	68	58	64	68	53	117	148
Sr	283	53	194	855	935	880	1210	760	745	202	840
Y	22	23	14	15	17	19	18	12	12	11	15
Zr	130	175	135	177	184	184	201	156	134	153	139
Nb	14.0	30.5	14.5	11.0	11.0	11.5	20.0	11.0	9.5	11.5	9.5
Pb	36	31	25	18	21	20		25	22	25	23
Th	15.6	22.0	13.4	10.8	10.4	9.8	6.4	10.0	9.4	10.8	11.0
U	4.4	5.0	4.4	2.6	3.6	2.0	1.8	2.6	2.2	3.6	3.6
V	14	5	8	77	91	125		73	75	18	66
Cr	4	<1	<1	125	119	208		43	53	2	42
Ni	4	2	5	72	67	105		31	29	4	26
Cu	6	3	6	33	34	49		25	9	6	22
Zn	27	39	32	65	71	81		63	57	48	68
Ce	69.87	93.95	81.73	80.76		92.99		77.30		69.11	68.07
Nd	29.98	29.11	28.37	35.72		40.21		29.61		22.16	28.91
Sm	5.62	4.61	4.58	6.20		7.18		5.14		3.79	5.02
Eu	1.08	0.585	0.858	1.63		1.83		1.36		0.863	1.34
Gd	4.43	3.73	3.38	4.68		5.47		3.80		2.85	3.78
Dy	3.73	3.78	2.76	3.27		4.05		2.56		2.14	2.80
Er	2.18	2.58	1.49	1.66		2.13		1.23		1.08	1.50
Yb	2.28	3.03	1.46	1.48		1.96		1.04		0.984	1.36

the basaltic-andesite unit can be approximated by up to 45% crystallization (53–59% SiO_2) using observed phenocrysts and proportions (sum $R^2 = 1.5$). Major element compositions of the augite andesite (e.g. 119, 64% SiO_2) can be approximated by 25% crystallization of the most silicic basaltic-andesite (59% SiO_2) using observed phenocrysts and proportions (sum $R^2 = 1.4$). In all the above cases the sum of residuals squared are higher than those expected for suites related by simple crystal fractionation. The most successful major element models relate the quartz latite (e.g. 116) and early rhyolite (e.g. 135B) by approximately 40% crystallization of the observed phenocrysts and proportions (sum $R^2 = 0.15$).

Major element fractionation models fail to relate either the Latir hornblende andesite or quartz latite to the basaltic-andesite, nor do they permit relating the quartz latite to mafic samples of hornblende andesite. Fractionation models do not permit relating the precaldera and caldera-related alkalic rocks to any of the metaluminous Latir rocks. Moreover, the comendite lavas are not crystal fractionates of intermediate-composition magmas similar to the alkalic dacite; plagioclase would probably be a major liquidus phase in the dacite during crystallization, and plagioclase fractionation cannot decrease CaO contents by a factor of 10 while maintaining relatively constant K_2O and Na_2O contents (Table 6). Finally, the major element compositions of the Miocene olivine andesite and hornblende andesite cannot be derived by crystal fractionation of any of the temporally and spatially associated basaltic lavas.

Trace elements. The concentrations of incompatible-elements such as Rb, Th, and U in the intermediate-composition Latir rocks can be explained by approximately 80% crystal fractionation of basalts with compositions similar to early-rift Hindsdale basalts exposed north of the Latir field (Lipman and Mehnert 1975; Thompson and Johnson 1987). This model assumes olivine + augite + plagioclase + / − hypersthene + / − hornblende fractionation using the results from major element crystal fractionation models. The elevated Pb contents of the Latir rocks requires addition of a crustal component, as previously discussed.

Plagioclase comprises approximately 50% of the pheno-

Table 6 (continued)

Xenocrystic andesite		Olivine basaltic-andesite		Alkalic dacite		Comendite		Outflow Amalia Tuff #1 Camp Creek Section Base		
118	123	81L-46	79L-14	106	114	141A	142	205W wr	204P pumice	41P pumice
63.6	62.6	53.4	55.8	65.3	65.7	72.4	70.3	77.4	76.5	77.4
1.04	0.78	1.50	1.87	0.91	1.05	0.39	0.43	0.13	0.08	0.10
14.3	15.2	14.3	14.5	14.7	16.7	12.8	14.5	11.7	12.6	12.0
5.30	3.59		9.49	6.17	4.38	4.31	4.23	1.84	1.11	
0.94	1.99		5.57	0.14	0.19	0.01	0.09	0.03	0.37	
5.75	5.25	10.20	4.48	5.73	4.15	3.91	3.91	1.69	1.37	1.47
0.06	0.07	0.13	0.12	0.07	0.12	0.14	0.06	0.04	0.03	<0.02
2.37	3.37	7.10	4.75	0.56	0.35	0.13	0.10	0.15	0.24	<0.10
4.35	5.09	7.80	7.24	4.06	4.08	0.91	0.60	0.36	0.58	0.09
4.01	3.77	3.00	3.35	3.90	4.08	3.98	4.25	3.69	2.77	3.90
4.01	3.50	2.20	1.97	4.36	3.17	5.25	5.75	4.83	5.91	5.04
0.51	0.37	0.42	0.36	0.42	0.51	0.07	0.07	<0.05	<0.05	<0.05
2.44	1.71	2.10	1.07	1.80	2.69	1.34	1.24	1.22	4.62	0.58
0.77	0.66	0.51	0.53	0.76	0.61	0.95	0.91	0.97	0.87	0.99
960	1310			1070	1160	450	520	110	54	24
88	103	36	88	82	58	82	92	125	203	152
745	930	688	849	376	482	24.5	25	47	46.5	5
16	18	15	9	39	42	54	47	56	89	49
187	181	132	177	330	360	795	865	284	221	357
17.5	11.0	9.0	16.0	25.0	27.5	26.0	28.0	37.0	54.0	43.0
18	22			12	12	16	19	23	34	18
11.4	10.4		5.3	8.6	8.4	13.6	15.8	16.8	20.5	17.4
3.2	1.4		1.0	2.2	3.0	4.4	5.6	3.4	8.8	3.2
95	93			6	6	<1	<1	9	3	3
151	107			<1	<1	<1	1	5	3	<1
55	57			3	4	2	2	2	3	1
37	33			4	3	4	5	6	5	4
76	69	104	80	97	143	111	115	129	176	112
95.41				104.7	112.4	212.0			48.88	124.3
44.24				50.16	53.58	93.07			31.78	63.41
7.30				10.21	10.96	15.02			11.25	12.84
1.79				2.76	3.05	2.10			0.134	0.369
5.36				9.25	9.93	11.97			12.51	9.82
3.36				7.95	8.67	10.49			15.61	9.56
1.57				4.26	4.53	5.95			9.71	5.52
1.29				3.83	4.00	5.68			9.04	5.31

crysts in the intermediate-composition Latir rocks, and this proportion is also indicated for parental basaltic magmas from major element fractionation models. This suggests that bulk Sr K_Ds were approximately unity throughout much of the fractionation sequence (e.g. Philpotts and Schnetzler 1970; Arth 1976; Henderson 1982). The Sr contents of the intermediate-composition Latir rocks probably, therefore, reflect those of their parental magmas unless substantial crustal Sr was added during assimilation.

Trace element fractionation models are most successful in relating the early rhyolite to parental magmas identical to the quartz latite. The Rb, Sr, Y, Zr, Nb, Th, U, and REE contents of the early rhyolite may be obtained by 40% crystallization of the quartz latite using observed phenocrysts and proportions (plagioclase > hornblende > biotite > > Fe-Ti oxides + sphene + zircon) and K_Ds appropriate for moderately silicic magmas (Arth 1976; Luhr and Carmichael 1980; Luhr et al. 1984; Nagasawa and Schnetzler 1971; Arth and Barker 1976; Henderson 1982).

Fractionation of olivine + augite + plagioclase + / − orthopyroxene + / − hornblende in basaltic parental magmas will uniformly increase the concentrations of all REEs unless large amounts of augite or hornblende are fractionated (> 60%) (Nagasawa and Schnetzler 1971; Schnetzler and Philpotts 1970; Arth 1976; Arth and Barker 1976; Luhr and Carmichael 1980; Henderson 1982). The HREE-depleted nature of the precaldera intermediate-composition Latir rocks (5 × CHOND) precludes derivation from magmas similar to the parental magmas of the postcaldera Latir rocks or the early-rift Hindsdale basalts (Fig. 8; Thompson et al. 1986; Thompson and Johnson 1987). The REE contents of the precaldera Latir rocks are also substantially different from those of the rift-related Miocene basalts described above and the Pliocene Servilleta Basalt (Fig. 8; Dungan et al. 1986).

Assimilation of bulk crust is unlikely in light of the low HREE contents of the precaldera Latir rocks because most crustal rocks have significantly higher HREE contents

Table 6 (continued)

	Outflow Amalia Tuff #1 Camp Creek Section Top			Peralkaline rhyolite		Miocene hornblende andesite		Miocene basalts		
	39 wr	134P pumice	27 vitrophyre	124 lava	127B lava	126	136	107	108	115
SiO_2	78.0	78.5	77.0	77.5	77.7	58.7	58.1	45.6	49.9	49.0
TiO_2	0.17	0.10	0.11	0.15	0.16	1.51	1.49	2.69	1.71	1.73
Al_2O_3	11.5	11.9	11.8	11.6	11.5	15.1	15.3	12.5	15.1	15.0
Fe_2O_3		1.68	0.84	1.32	1.39	6.73	6.58	7.22	3.94	5.32
FeO		0.06	0.90	0.22	0.20	0.97	1.27	4.59	7.70	6.92
FeO_{TOTAL}	1.24	1.58	1.65	1.41	1.46	7.09	7.25	11.22	11.38	11.86
MnO	0.10	<0.02	0.04	0.11	0.10	0.12	0.08	0.16	0.16	0.18
MgO	<0.10	0.17	<0.10	<0.10	<0.10	2.85	3.52	8.65	7.94	8.66
CaO	0.06	0.19	0.49	<0.10	0.06	6.36	6.22	11.93	8.66	8.72
Na_2O	4.27	2.13	4.12	4.35	4.37	4.48	4.28	3.80	3.47	3.30
K_2O	4.68	5.36	4.85	4.80	4.71	3.19	3.18	1.58	1.32	1.13
P_2O_5	<0.05	<0.05	<0.05	<0.05	<0.05	0.56	0.56	1.95	0.39	0.39
LOI	0.77	1.83	3.61	0.58	0.53	1.42	1.55	5.59	2.05	2.21
AI	1.05	0.78	1.02	1.06	1.07	0.72	0.68	0.64	0.47	0.44
Ba	44	115	8	8	12	1180	1150	1630	470	455
Rb	110	152	134	156	144	48.5	44	20.5	24	19.5
Sr	7.5	49	16	1.5	4	1570	1750	1820	575	530
Y	46	45	68	53	61	15	15	18	19	20
Zr	378	333	350	483	515	186	172	219	129	119
Nb	37.0	35.5	40.0	48.0	46.0	25.5	26.0	69.0	18.5	16.5
Pb	21	19	29	19	26	12	14	9	6	3
Th	16.2	18.6	17.4	21.5	22.0	4.4	6.4	7.2	3.0	3.8
U	4.0	5.0	5.4	4.8	7.6	2.8	2.0	2.2	<0.2	<0.2
V	3	4	<1	3	2	101	119	189	150	155
Cr	<1	<1	<1	1	<1	51	61	213	210	220
Ni	<1	<1	<1	<1	<1	39	42	152	128	137
Cu	<1	3	4	2	5	57	39	52	41	43
Zn	102	121	161	143	122	90	98	126	100	104
Ce	78.62		158.3			97.88	99.36	142.9	46.14	42.78
Nd	38.07		68.25	17.58		42.55	42.65	69.66	24.01	22.57
Sm	10.13		14.45	5.20		6.97	7.04	11.37	5.37	5.06
Eu	0.604		0.410	0.357		1.87	1.84	2.99	1.82	1.70
Gd	8.99		12.77	6.12		5.03	5.02	7.70	5.34	5.01
Dy	10.24		12.91	9.13		3.23	3.26	4.43	4.63	4.50
Er	5.91		7.58	6.27		1.46	1.52	1.83	2.40	
Yb	5.48		7.10	6.53		1.19	1.25	1.42	2.05	1.92

Major and most trace-elements by wave-length dispersive XRF. Ferrous Fe by titration. REEs by IDMS. "LOI" = loss on ignition. "AI" = agpaitic index. Analyses normalized to 100% anhydrous using total Fe as FeO

(> 15 × CHOND; Haskin et al. 1968). Assimilation/mixing of partial melts derived from crust with residual garnet (or possibly clinopyroxene) would, however, provide a HREE-depleted crustal component.

The high Y, Zr, and REE contents of the alkali dacite, comendite, Amalia Tuff, and peralkaline rhyolite cannot be obtained by crystal fractionation of any metaluminous Latir rocks. Coupled assimilation/crystallization cannot produce the high trace element contents of the alkalic rocks if average crustal compositions are considered (Taylor 1964).

Crystal fractionation of the alkalic dacite to produce the comendite requires substantial apatite crystallization to lower P_2O_5 contents by a factor of 6 (Table 6), and this would deplete the REE contents in the comendite, which is opposite of what is observed. Moreover, large differences in Sr and Pb isotope ratios between the two units suggest that they are not genetically related even if assimilation occurred (Johnson and Lipman submitted).

Trace element variations between the comendite and early-erupted portions of the Amalia Tuff may be explained by 50% crystallization of sanidine and arfvedsonite in approximately 4:1 proportions. In addition, 0.02% zircon and 0.06% allanite fractionation is required to match Zr and REE variations, respectively. Zircon is present in the comendite, although allanite has not been found in thin section. Large differences in Sr isotope ratios, however, suggest that the two units are not related by simple crystal fractionation (Johnson and Lipman submitted).

Alkalic rocks

Origin. The relation between silicic and mafic alkalic rocks and associated metaluminous rocks has been extensively

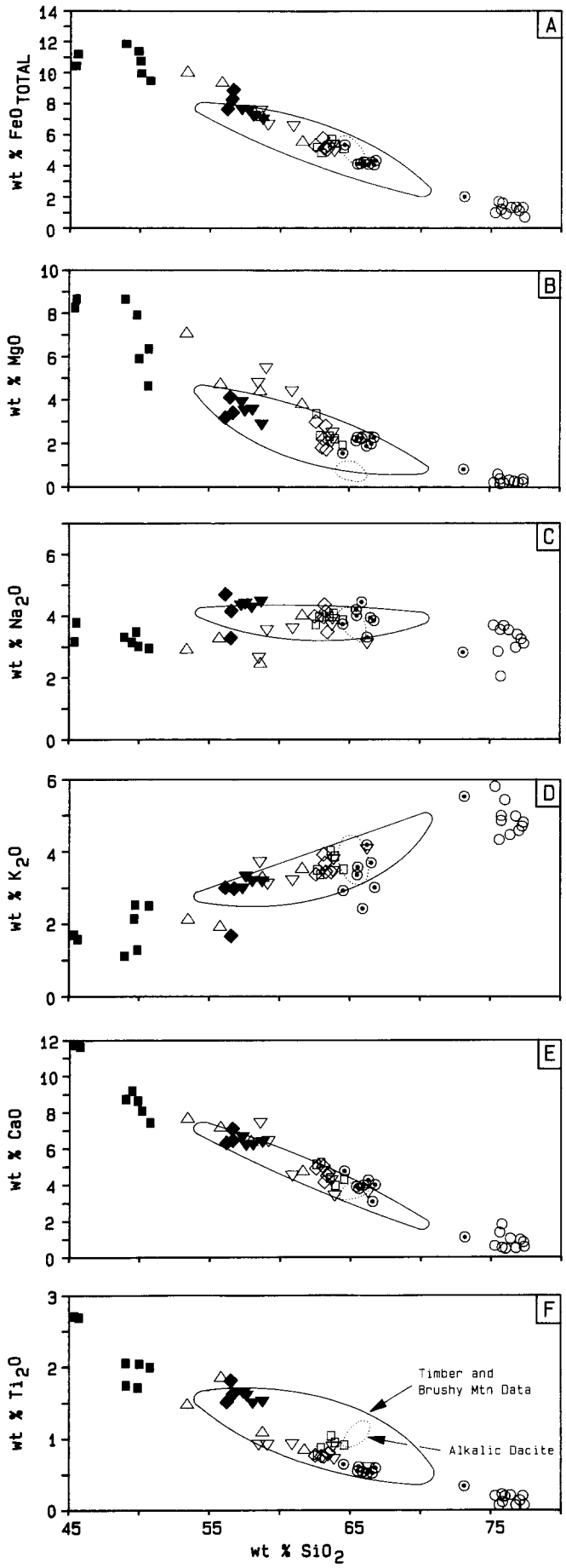

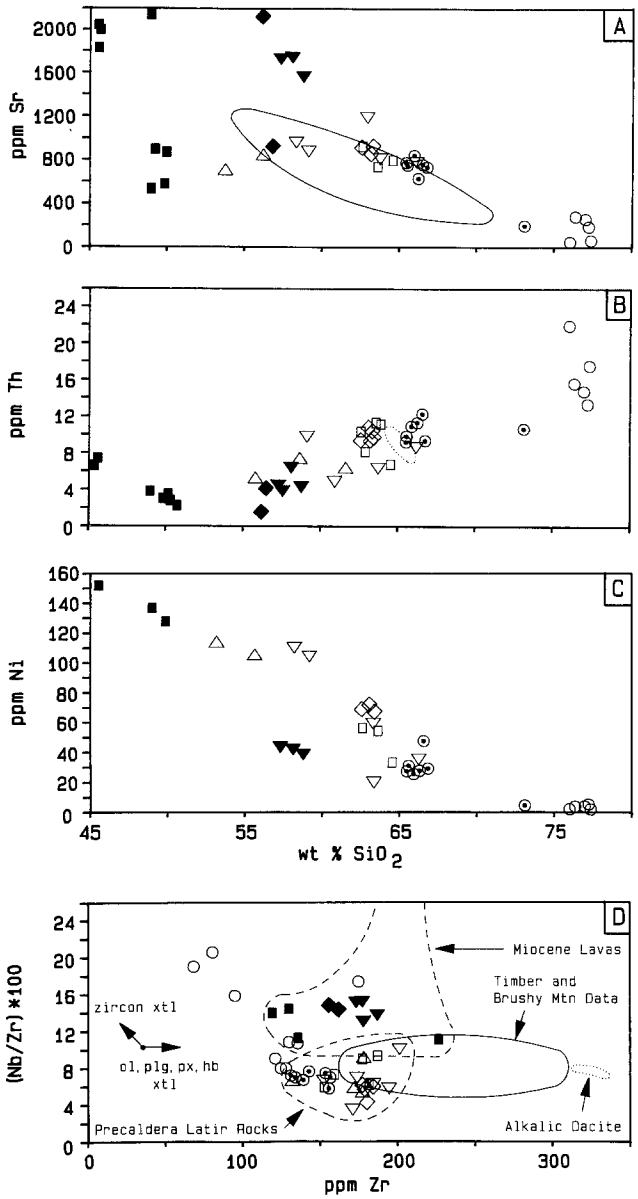

Fig. 7A–D. Selected trace element compositions of for metaluminous precaldera Latir rocks and Miocene lavas. Symbols as in Fig. 6. *Arrows* in Nb-Zr diagram illustrate relative paths taken by zircon, olivine, plagioclase, pyroxene, and hornblende fractionation. Note that variations in Nb/Zr ratios of the early rhyolite may be explained by slight zircon fractionation, whereas Nb/Zr ratio variations in more mafic rocks probably reflect variations in parental magma compositions

Fig. 6A–F. Major element compositions of metaluminous precaldera Latir rocks and Miocene lavas. *Dotted outline* indicates field of data for alkalic dacite unit. *Solid outline* indicates field of post-caldera Latir lavas exposed in the Timber and Brushy Mountains (data from Thompson et al. 1986). ○ early rhyolite. ◇ augite andesite. ▽ Latir hornblende andesite. ⊙ Latir Peak Quartz Latite. □ xenocrystic andesite. △ olivine basaltic-andesite. ■ Miocene basalt. ◆ Miocene olivine andesite. ▼ Miocene hornblende andesite

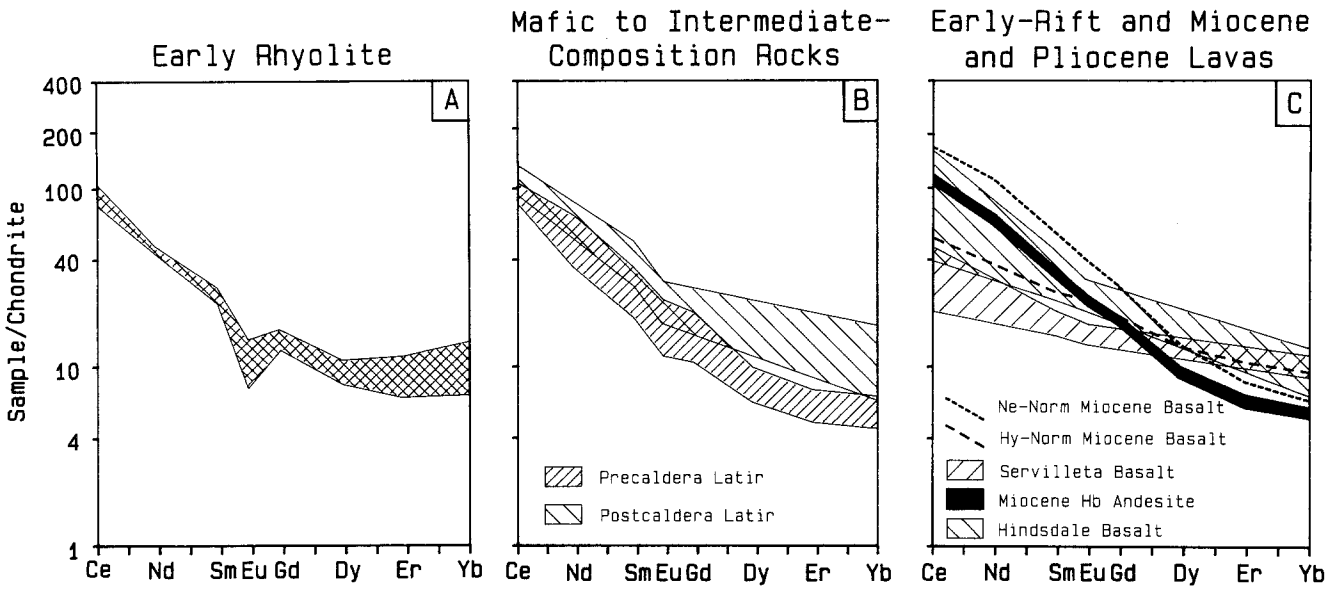

Fig. 8A–C. Rare Earth Element (REE) compositions of **A**: early rhyolite, **B**: precaldera (this study) and postcaldera (Thompson et al. 1986) intermediate-composition Latir rocks, and **C**: Miocene lavas, early-rift Hindsdale lavas (Thompson and Johnson 1987), and Servilleta Basalt (Dungan et al. 1986). Chondrite normalization used values by Masuda et al. (1973) multiplied by 1.2 to approximate those of Haskin et al. (1968)

debated. Crystal fractionation has been proposed for alkalic suites in the East African Rift and oceanic settings (Macdonald 1974a, 1974b; Macdonald et al. 1974; Weaver 1976; Harris 1983; Wolff and Storey 1984; Baker 1987). Some workers suggest that volatile transport of alkalis and other elements is important in the evolution of silicic alkalic rocks, based in part on experimental data (Bailey 1974a; Bailey and Macdonald 1975; Martin 1974; Kogarko 1974; Barker 1976; Hards 1976) and also chemical variations in volcanic centers (Mahood 1981; Taylor et al. 1981; Leat et al. 1984). Bailey (1974b, 1980) argues that some silicic alkalic rocks are derived by melting continental crust in the presence of degassing alkalic basalts. Isotopic data have identified crustal components in some alkalic rocks, and this has been ascribed to coupled crystal fractionation/assimilation processes (Norry et al. 1980; Downes 1984). Assimilation of crustal rocks has been invoked as the driving force toward silica-saturation during differentiation of undersaturated mafic magmas (Downes 1984; Fitton 1987).

We interpret the alkalic dacite lavas as products of coupled crystal fractionation/assimilation of alkali basalts that did not reach the surface. The alkalic dacite, comendite, and Amalia Tuff, however, are not related by simple crystal fractionation or coupled crystal fractionation/assimilation from a single parental magma.

Katophoritic to richteritic amphibole cores are always rimmed by arfvedsonitic amphibole in the resurgent peralkaline granite that is cogenetic with the Amalia Tuff. Moreover, portions of calcic amphibole cores and rare biotite phenocrysts are replaced by tetrasilicic mica (Czamanske and Dillet 1988). These relations suggest that the Amalia Tuff magma was derived from a more Ca- and Al-rich magma that evolved to peralkaline compositions. Cores of some sphenes in resurgent metaluminous granites have high-Na and low-Al contents, notably characteristic of sphene in the peralkaline granite, indicating that metaluminous and peralkaline magmas were closely associated during caldera formation.

We suggest that the silicic peralkaline rocks are the result of fractionation of trace element-enriched metaluminous magmas that contained large crustal components. Coupled crystal fractionation/assimilation alone does not explain the fact that the most radiogenic Sr and Pb isotope ratios in the Latir field are in the most alkaline rocks. Contamination with silica-saturated crust should produce a *decrease* in alkalinity, as suggested by the studies of Downes (1984) and Fitton (1987). If, however, volatiles are important in transporting alkalis and other elements, the trace element-enriched nature of the parental metaluminous magmas may be largely a consequence of degassing of underlying water- and halogen-rich alkali basalt magmas into an overlying silicic magma chamber. Protracted fluxing by water and halogens may have driven the metaluminous magmas toward peralkaline compositions. Trace element-enriched metaluminous granites, similar to the "A-type" granites described by Collins et al. (1982), underlie the peralkaline granites in the Questa caldera, and may be similar to the magmas that were parental to the Amalia Tuff. Both metaluminous and peralkaline Latir rocks contain normative quartz, and relatively minor changes in alkali contents would be required to derive the peralkaline magmas from metaluminous parental magmas.

Although the elevated trace element contents of the silicic peralkaline Latir rocks could, in principle, be derived by partial melting of most crustal rocks without invoking a special role for volatile transport, this explanation is unsatisfactory. The Zr contents of the comendites could, for example, be explained by 10% batch or fractional melting of crust with typical Zr abundances (150 ppm; Taylor 1964) if zircon melts completely under hydrous conditions (Harrison and Watson 1983). Such a model does not, however, explain the relative rarity of trace element-enriched magmas, such as silicic peralkaline rocks (Macdonald and Bailey 1973). If the silicic peralkaline rocks were derived by crustal melting, melting probably occurred in the presence of high water- and halogen-fluxes.

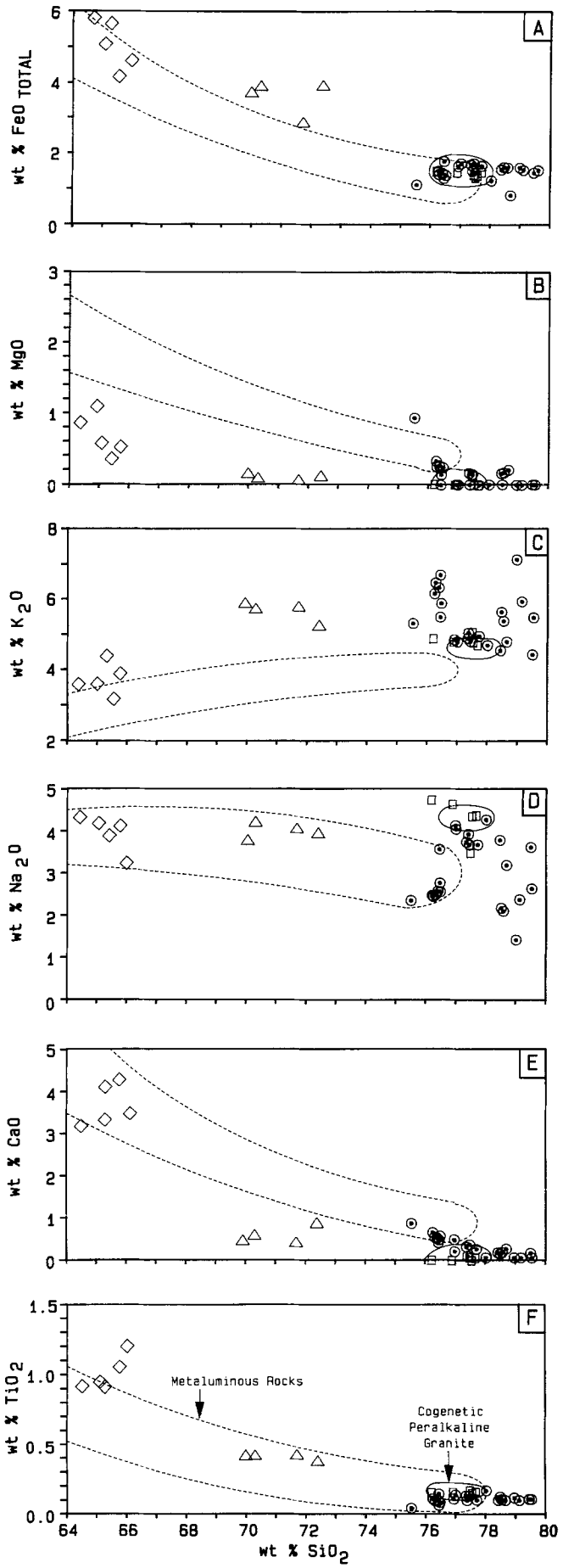

Amalia Tuff zonation. The Amalia Tuff is zoned in mineralogy and most trace elements but relatively homogeneous in major element compositions. Although interpretation of the magmatic gradients is complicated by incomplete preservation of tuff sections, limited preservation of collectable pumice, and groundmass devitrification and alkali exchange, the reconstructed compositional gradients can be largely accounted for by fractionation of observed phenocryst phases, including accessory minerals. Less than 0.1% allanite fractionation would produce the roofward LREE depletion in the tuff (Mahood and Hildreth 1983), but this would deplete Th roofward, which is opposite to the observed trends (Fig. 12). Small amounts of sphene fractionation (<0.5%) are permissible (Luhr et al. 1984), but this would deplete Th roofward. Apatite fractionation is unlikely due to its scarcity in the tuff and is inconsistent with a cross-over in REE variations between Eu and Gd (Fig. 12). Zircon fractionation (<0.1%) can explain the roofward depletion of Zr, although even small amounts would significantly decrease Nb, Th, and HREEs. Simultaneous fractionation of several accessory minerals is probable, and this requires increased sanidine and quartz fractionation to enrich Y, Nb, HREEs, Th, and U roofward.

Roofward depletion of Eu can be explained by sanidine fractionation, although reasonable sanidine/quartz ratios require at least 50% crystallization using relatively high mineral/melt K_Ds. To reconcile the observed roofward increase in Y, Nb, HREEs, Pb, and U with the amount of accessory phase fractionation suggested above requires at least 75% crystallization of sanidine and quartz across the compositional range of the #1 Camp Creek tuff section. If the magmatic zonation extended beyond that sampled at this one outflow locality, then even greater amounts of crystallization would be required. Crystal settling as a mechanism is inconsistent with variations in observed mineralogy (ie: the lack of allanite in the late-erupted portions of the Amalia Tuff). While the trace element zonation may be due to crystal fractionation, such fractionation most likely occurred below the level tapped by the caldera-forming eruption. In addition, liquid-state differentiation mechanisms may have been involved in establishing some trace element gradients (Hildreth 1979; 1981).

Summary and conclusions

Magmatism of the Latir volcanic field evolved in an open system that included crystal fractionation, magma mixing, crustal assimilation, and volatile-transport differentiation. Initial magmatism (28.5 Ma), dominated by metaluminous high-SiO_2 rhyolite, was the product of protracted crystallization from intermediate-composition parental magmas that had not reached the surface. These early intermediate-composition magmas had undergone extensive assimilation/fractional crystallization and probably had compositions similar to those of the voluminous quartz latite erupted after the early rhyolite.

Fig. 9 A–F. Major element compositions of precaldera and caldera-related alkalic Latir rocks. *Dashed outline* indicates field of data of metaluminous precaldera rocks from Fig. 6. *Solid outline* indicates field of data for peralkaline granite that is cogenetic with the Amalia Tuff (Johnson et al. submitted). ⊙ Amalia Tuff. □ peralkaline rhyolite. △ comendite. ◇ alkalic dacite

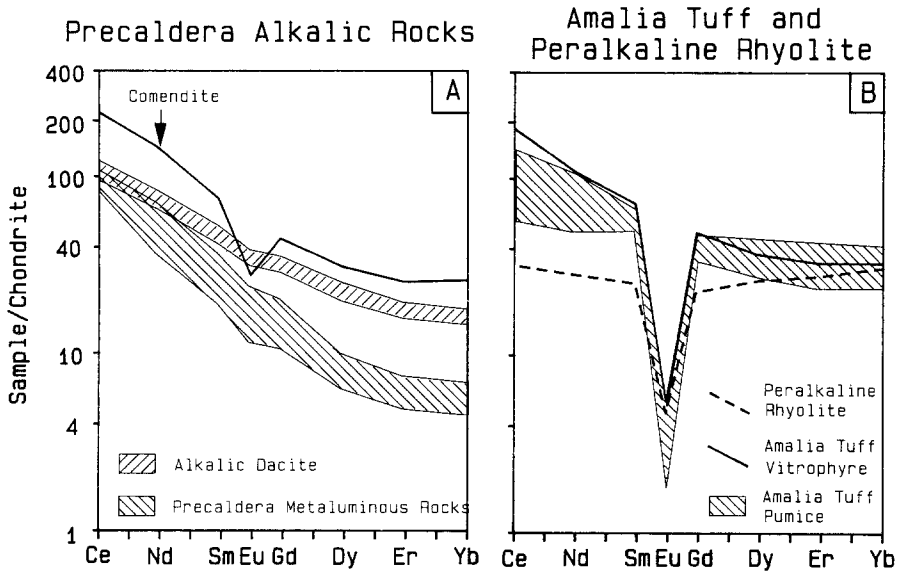

Fig. 10A, B. REE compositions of precaldera and caldera-related alkalic Latir rocks. Also shown for comparison is outline of data for precaldera metaluminous rocks from Fig. 8. Normalization as in Fig. 8

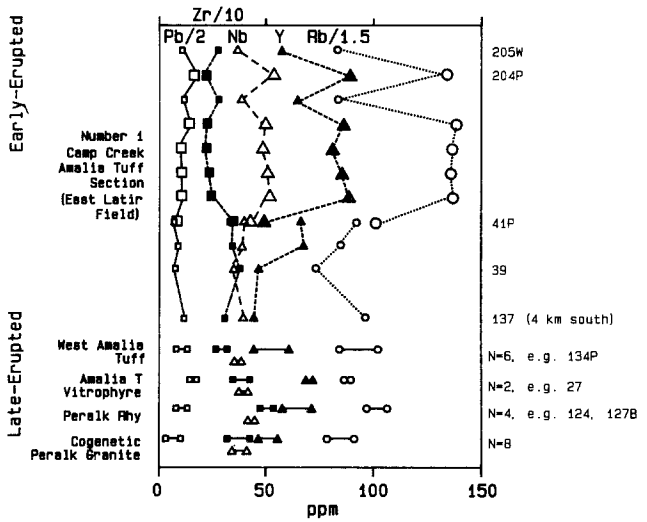

Fig. 11. Variation of selected trace elements with inverse stratigraphic position in the Amalia Tuff and cogenetic units. *Small symbols* represent whole-rock (bulk-tuff) samples, whereas *large symbols* represent pumice samples. Pb, Zr, and Rb concentrations divided by 2, 10, and 1.5, respectively, for plotting purposes

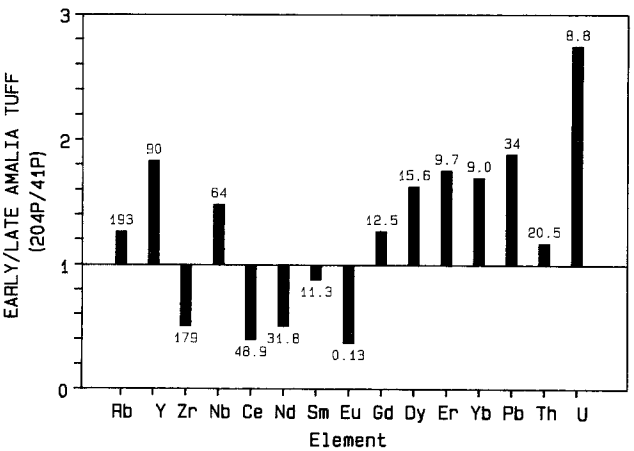

Fig. 12. Enrichment-factor diagram for samples from the top and bottom of non-welded, pumice zone at #1 Camp Creek section. Concentrations in early-erupted tuff sample 204P shown *above/below bars*

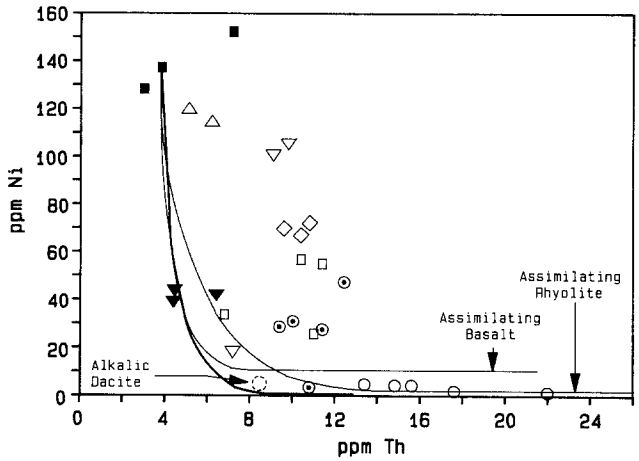

Fig. 13. Ni-Th variations for metaluminous precaldera Latir rocks and Miocene lavas. Symbols as in Fig. 6. *Heavy line* indicates Ni and Th variations during crystal fractionation of olivine, plagioclase, and augite from sample 115, with fractionation ending at 70%. Coupled assimilation (mixing)/fractional crystallization curves calculated using assimilation to crystallization rates of 1:2 are also shown for basalt and rhyolite assimilation (mixing). "Assimilating Basalt" curve ends at 70% crystallization, and "Assimilating Rhyolite" curve intersects the edge of the diagram at approximately 50% crystallization

Early rhyolite volcanism was quickly followed by eruption of metaluminous intermediate-composition lavas of varied phenocryst mineralogy. The metaluminous rocks can be broadly divided into three suites: 1) a volumetrically-dominant H_2O-rich suite that includes the precaldera hornblende andesite and quartz latite, 2) a relatively dry and presumably high-temperature suite that includes the olivine basaltic-andesite and augite andesite, and 3) a mineralogically-complex suite of xenocryst-rich lavas (xenocrystic andesite). All rock types are variably enriched in MgO, Ni, and Cr contents over those expected for intermediate-composition rocks, suggesting that most rocks are the products of mixing between fractionated magmas and relatively primitive magmas. Virtually all of the intermediate-composition lavas contain large crustal components.

Intermediate to silicic alkalic magmatism began during

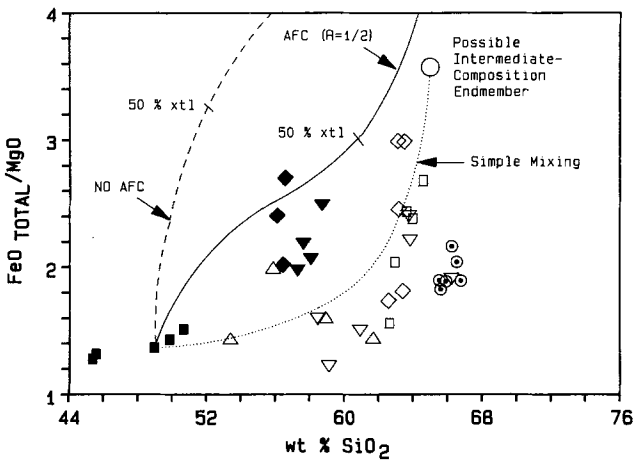

Fig. 14. FeO_{Total}/MgO variations for metaluminous precaldera Latir rocks and Miocene lavas. Symbols as in Fig. 6. *Heavy-dashed curve* indicates low-pressure crystallization trend of basalt 115 calculated using EQUIL (Nielson 1985). *Solid curve* indicates coupled assimilation/fractional crystallization (AFC) with a assimilation to crystallization ratio (R) of 1:2. The silicic component used in the calculations is early rhyolite 135B. Simple mixing is also illustrated between the basalt endmember and a hypothetical, evolved intermediate-composition magma

initial regional extension in northern New Mexico, consistent with observations in other extensional settings (Macdonald 1974b; Noble and Parker 1974; Rytuba and McKee 1984). The shift to alkaline magmatism probably reflects a change in the composition of basalts injected into the crust to more alkaline compositions. The silicic peralkaline rocks, such as the Amalia Tuff, fractionated from trace element- and alkali-enriched metaluminous magmas that contain large crustal components. Crustal melting or assimilation/fractional crystallization involving degassing, water- and halogen-rich alkali basalts may have been the fundamental driving force for increasing trace element and alkali contents in the silicic magmas to produce peralkaline compositions. This model is consistent with a genetic link between silicic peralkaline magmas and associated mafic alkalic magmas, but does not require derivation of the silicic magmas solely by crystal fractionation of mafic magmas.

Trace element variations in the Amalia Tuff can be explained by 75% crystal fractionation of observed phenocrysts. Crystal settling is inconsistent with observed variations in mineralogy, and crystallization is envisioned to have occurred at a level below that tapped by the caldera-forming eruption (e.g. Baker and McBirney 1985).

Crustal assimilation and magma mixing, documented for the intermediate-composition Latir rocks, were not important processes in the evolution of the spatially related Miocene lavas. The relatively closed system behavior of the Miocene lavas may be a consequence of evolution during active block faulting in northern New Mexico during the Miocene, in contrast to the incipient rifting that occurred at 26 Ma (e.g. Kelley and Duncan 1986). Incompatible-element ratios and REE patterns of the Miocene lavas, however, indicate that the Ne- and Hy-normative basalts, olivine andesites, and hornblende andesites were derived from distinct parental magmas.

The close association of mixing involving primitive magmas and crustal contamination in the Latir magmas contrasts with the minimal extent to which these processes occurred in the Miocene lavas. We suggest that the requirements for mixing and extensive contamination processes are basically the same, namely development of relatively large magma chambers in the crust that are sustained by large basalt fluxes from the mantle. A relatively low basalt flux from the mantle or tectonic setting that did not allow large volumes of basalt to pool in the crust, such as rapid extension (Johnson and O'Neil 1984), during the Miocene may explain the lack of extensive crustal contamination and mixing in the younger lavas.

Acknowledgments. We thank A. Grunder, J. Hagstrum, D. Sawyer, and J. Wooden for helpful discussions. R. Coleman, G. Czamanske, G. Mahood, and R. Thompson reviewed earlier versions of the manuscript; C. Bacon is thanked for particularly helpful reviews. J. Luhr and an anonymous reviewer provided journal reviews. M. Pernokas assisted with sample preparation. B. Chappell and G. Hanson cheerfully provided access to their laboratories, and J. O'Neil, J. Stacey, and J. Wooden are thanked for their strong support of geochemistry in Menlo Park. Material support was provided by the U. S. Geological Survey, fellowships to C.M.J. from the National Science Foundation, State of California, and Stanford University, and a Stanford University McGee Research Grant to C.M.J.

References

Arth JG (1976) Behavior of trace elements during magmatic processes – a summary of theoretical models and their applications. J Res US Geol Surv 4:41–47

Arth JG, Barker F (1976) Rare-earth partitioning between hornblende and dacitic liquid and implications for the genesis of trondhjemitic-tonalitic magmas. Geology 4:534–536

Bacon CR (1986) Magmatic inclusions in silicic and intermediate volcanic rocks. J Geophys Res 91:6091–6112

Bacon CR, Metz J (1984) Magmatic inclusions in rhyolites contaminated by basalts and compositional zonation beneath the Coso volcanic field California. Contrib Mineral Petrol 85:346–365

Bailey DK (1974a) Experimental petrology relating to oversaturated peralkaline volcanics: a review. Bull Volcanol 38:637–652

Bailey DK (1974b) Origin of alkaline magmas as a result of anatexis-melting in the deep crust. In: Sorensen H (ed) The alkaline rocks. John Wiley and Sons, London, pp 436–441

Bailey DK (1980) Volcanism, Earth degassing and replenished lithospheric mantle. Phil Trans Roy Soc Lond A297:309–322

Bailey DK, Macdonald R (1975) Fluorine and chlorine in peralkaline liquids and the need for magma generation in an open system. Miner Mag 40:405–414

Baker BH (1987) Outline of the petrology of the Kenya rift alkaline province. In: Fitton JG, Upton BG (eds) Alkaline igneous rocks, The Geological Society, Blackwell, Oxford, pp 293–312

Baker BH, McBirney AR (1985) Liquid fractionation. Part III: geochemistry of zoned magmas and the compositional effects of liquid fractionation. J Volcanol Geotherm Res 24:55–81

Barker DS (1976) Phase relations in the system $NaAlSiO_4$-SiO_2-NaCl-H_2O at 400°–800° C and 1 kilobar, and petrologic implications. Jour Geol 84:97–106

Brown WL, Parsons I (1981) Towards a more practical two-feldspar geothermometer. Contrib Mineral Petrol 76:369–377

Butler AP Jr (1971) Tertiary volcanic stratigraphy of the eastern Tusas Mountains, southwest of the San Luis Valley, Colorado-New Mexico, New Mexico Geol Soc Guidebk 22:289–300

Clark KF, Read CB (1972) Geology and ore deposits of the Eagle Nest area, New Mexico. New Mexico Bur Mines Miner Res Bull 94, 152 pp

Collins WJ, Beans SD, White AJR, Chappell BW (1982) Nature and origin of A-type granites with particular reference to southeastern Australia. Contrib Mineral Petrol 80:189–200

Czamanske GK, Shunso I, Atkin SA (1981) Chemistry of rock-forming minerals of the Cretaceous-Paleocene batholith in southwestern Japan and implications for magma genesis. J Geophys Res 86:10431–10469

Czamanske GK, Dillet B (1988) Alkali amphibole, tetrasilicic mica, and sodic pyroxene in peralkaline siliceous rocks, Questa caldera, New Mexico. Amer J Sci (in press)

DePaolo DJ (1981) Trace-element and isotopic effects of combined wall rock assimilation and fractional crystallization. Earth Planet Sci Lett 53:189–202

DePaolo DJ, Johnson RW (1979) Magma genesis in the new Britain island-arc: constraints from Nd and Sr isotopes and trace-element patterns. Contrib Mineral Petrol 70:367–379

Dillet B, Czamanske GK (1987) Aspects of the petrology, mineralogy, and geochemistry of the granitic rocks associated with Questa caldera, northern New Mexico. US Geol Surv Open-File Report 87-258 228 pp

Downes H (1984) Sr and Nd isotope geochemistry of coexisting alkaline magma series, Cantal, Massif Central, France. Earth Planet Sci Lett 69:321–334

Dungan MA, Lindstrom MM, McMillan NJ, Moorbath S, Hoefs J, Haskin LA (1986) Open system magmatic evolution of the Taos Plateau volcanic field, northern New Mexico – I: the petrology and geochemistry of the Servilleta Basalts. J Geophys Res 91:5999–6028

Eichelberger JC (1978) Andesitic volcanism and crustal evolution. Nature 275:21–27

Fitton JG (1987) The Cameroon line, West Africa: a comparison between oceanic and continental alkaline volcanism. In: Fitton JG, Upton BGJ (eds) Alkaline Igneous Rocks, The Geological Society, Blackwell, Oxford, pp 273–292

Gilbert MC, Helz RT, Poop RK, Spear FS (1982) Experimental studies of amphibole stability. In: Veblen DR, Ribbe PH (eds) Reviews in mineralogy 9B: Amphiboles: petrology and experimental phase relations, Mineral Soc Amer, pp 229–354

Grove TL, Baker MB (1984) Phase equilibrium controls on the tholeiitic verses calc-alkaline differentiation trends. J Geophys Res 89:3253–3274

Hagstrum JT, Lipman PW (1986) Paleomagnetism of the structurally deformed Latir volcanic field, northern New Mexico: relations to formation of the Questa caldera and development of the Rio Grande rift. J Geophys Res 91:7383–7402

Hards N (1976) Distribution of elements between the fluid phase and silicate melt phase of granites and nepheline syenites. NERC Pub Serie D, pp 88–90

Harris C (1983) The petrology of lavas and associated plutonic inclusions of Ascension Island. J Petrol 24:424–470

Harrison TM, Watson EB (1983) Kinetics of zircon dissolution and zirconium diffusion in granitic melts of variable water content. Contrib Mineral Petrol 84:66–72

Haskin LA, Haskin MA, Frey FA, Wildeman (1968) Relative and absolute terrestrial abundances of the rare earths. In: Ahrens LH (ed) Origin and distribution of the elements, Pergamon, Oxford, pp 889–912

Helz RT (1973) Phase relations of basalts in their melting range at P $H_2O = 5$ Kb as a function of oxygen fugacity. Part I. Mafic phases. J Petrol 14:249–302

Helz RT (1976) Phase relations of basalts in their melting range at PH20 = 5 Kb. Part II. Melt compositions. J Petrol 17:139–193

Henderson P (1982) Inorganic geochemistry. Pergamon, Oxford, 353 pp

Hildreth W (1979) The Bishop Tuff: evidence for the origin of compositional zonation in silicic magma chambers. Geol Soc Amer Spec Pap 180:43–75

Hildreth W (1981) Gradients in silicic magma chambers: implications for lithospheric magmatism. J Geophys Res 86:10153–10192

Huppert HE, Sparks RSJ, Whitehead JA, Hallworth MA (1986) Replenishment of magma chambers by light inputs. J Geophys Res 91:6113–6112

Johnson CM, O'Neil JR (1984) Triple junction magmatism: a geochemical study of Neogene volcanic rocks in western California. Earth Planet Sci Lett 71:241–262

Kelley SA, Duncan IJ (1986) Late Cretaceous to middle Tertiary tectonic history of the northern Rio Grande rift. J Geophys Res 91:6246–6262

Kogarko LN (1974) Role of volatiles. In: Sorensen H (ed) The alkaline rocks, John Wiley and Sons, London, pp 474–487

Koyaguchi T (1986a) Evidence for two-stage mixing in magmatic inclusions and rhyolitic lave domes on Niijima Island, Japan. J Volcanol Geotherm Res 29:71–98

Koyaguchi T (1986b) Textural and compositional evidence for magma mixing and its mechanism, Abu volcano group, southwestern Japan. Contrib Mineral Petrol 93:33–45

Leat PT, Macdonald R, Smith RL (1984) Geochemical evolution of the Menengai caldera volcano, Kenya. J Geophys Res 89:8571–8592

Lindsley DH (1983) Pyroxene geothermometry. Amer Mineral 68:477–493

Lipman PW (1983) The Miocene Questa caldera, northern New Mexico: relation to batholith emplacement and associated molybdenum mineralization. In: The genesis of Rocky Mountain ore deposits: changes with time and tectonics, Proc Denver Region Explor Geol Soc Symp, pp 133–147

Lipman PW (1988) Evolution of silicic magma in the upper crust: the mid-Tertiary Latir volcanic field and its cogenetic granitic batholith, northern New Mexico, USA. In: The origin of granites. Trans Royal Soc Edinburg (in press)

Lipman PW, Mehnert HH (1975) Late Cenozoic basaltic volcanism and development of the Rio Grande depression in the southern Rocky Mountains. In: Curtis BF (ed) Geologic history of the southern Rocky Mountains. Geol Soc Amer Mem 144:119–154

Lipman PW, Reed JC Jr (1988) Geologic map of the Latir volcanic field and adjacent areas, northern New Mexico. US Geol Survey Misc Invest Map I-1907 (in press)

Lipman PW, Mehnert HH, Naeser CW (1986) Evolution of the Latir volcanic field, northern New Mexico and its relation to the Rio Grande rift, as indicated by K-Ar and fission-track dating. J Geophys Res 91:6329–6346

Lipman PW, Doe BR, Hedge CE, Steven TA (1978) Petrologic evolution of the San Juan volcanic field, southwestern Colorado: Pb and Sr isotope evidence. Geol Soc Amer Bull 89:59–82

Luhr JF, Carmichael ISE (1980) The Colima volcanic complex, Mexico: I. Post-caldera andesites from Volcan Colima. Contrib Mineral Petrol 71:343–372

Luhr JF, Carmichael ISE, Varekamp JC (1984) The 1982 eruptions of El Chichon volcano, Chiapas, Mexico: mineralogy and petrology of the anhydrite-bearing pumices. J Volcanol Geotherm Res 23:69–108

Macdonald R (1974a) The role of fractional crystallization in the formation of the alkaline rocks. In: Sorensen H (ed) The Alkaline Rocks, John Wiley and Sons, London, pp 442–458

Macdonald R (1974b) Tectonic settings and magma associations. Bull Volcan 38:575–593

Macdonald R, Bailey DK (1973) The chemistry of the peralkaline oversaturated obsidians. US Geol Surv Prof Pap 440-N-1:1–37

Macdonald R, Bailey DK, Barberi F (1974) Recommendations for further studies on the peralkaline oversaturated volcanic rocks. Bull Volcan 38:828–836

Mahood GA (1981) Chemical evolution of a Pleistocene rhyolite center; Sierra La Primavera, Jalisco, Mexico. Contrib Mineral Petrol 77:129–149

Mahood G, Hildreth W (1983) Large partition coefficients for trace elements in high-silica rhyolites. Geochim Cosmochim Acta 47:11–30

Manley K (1981) Redefinition and description of the Los Pinos Formation of northcentral New Mexico. Geol Soc Amer Bull 92:984–989

Martin RF (1974) Role of water in pantellerite genesis. Bull Volcanol 38:666–679

Masuda AW, Nakamura H, Tanaka T (1973) Fine structure of

mutually normalized rare-earth patterns of chondrites. Geochim Cosmochim Acta 37:239–248
McKinlay PF (1956) Geology of Costilla and Latir Peak quadrangles, Taos County, New Mexico. NM Bur Mines Min Res Bull 42, 32 pp
McKinlay PF (1957) Geology of the Questa quadrangle, Taos County, New Mexico. NM Bur Mines Min Res Bull 53, 23 pp
McMillan NJ, Dungan MA (1986) Magma mixing as a petrogenetic process in the development of the Taos Plateau volcanic field, New Mexico. J Geophys Res 91:6029–6045
Miyashiro A (1974) Volcanic rock series in island arcs and active continental margins. Am J Sci 274:321–355
Nagasawa H, Schnetzler CC (1971) Partitioning of rare earth, alkali and alkaline earth elements between phenocrysts and acidic igneous magma. Geochim Cosmochim Acta 35:953–968
Nash WP, Crecraft HR (1985) Partition coefficients for trace elements in silicic magmas. Geochim Cosmochim Acta 49:2309–2322
Nielson RL (1985) EQUIL: a program for the modeling of low-pressure differentiation processes in natural mafic magma bodies. Comput Geosci 11:531–546
Noble DC, Parker DF (1974) Peralkaline silicic volcanic rocks of western United States. Bull Volcanol 38:803–827
Norry MJ, Truckle PH, Lippard SJ, Hawkesworth CJ, Weaver SD, Marriner GF (1980) Isotopic and trace element evidence from lavas, bearing on mantle heterogeneity beneath Kenya. Phil Trans Roy Soc Lond A 297:259–271
Novak SW, Bacon CR (1986) Pliocene volcanic rocks of the Coso Range, Inyo County, California. US Geol Surv Prof Paper 1383
Papike JJ, Cameron KL, Baldwin K (1974) Amphiboles and pyroxenes: characterization of other than quadrilateral components and estimates of ferric iron from microprobe data. Geol Soc Amer Abs Prog 6:1053–1054
Philpotts RA, Schnetzler CC (1970) Phenocryst-matrix partition coefficients for K, Rb, Sr and Ba, with applications to anorthosite and basalt genesis. Geochim Cosmochim Acta 34:307–322
Reed JC Jr, Lipman PW, Robertson JR (1983) Geologic map of the Latir Peak and Wheeler Peak wildernesses and Columbine-Hondo wilderness study area, Taos County, New Mexico. US Geol Surv Misc Field Studies Map MF-1570-B
Robert JL, Maury RC (1979) Natural occurrence of a (Fe, Mn, Mg) tetrasilicic potassium mica. Contrib Mineral Petrol 68:117–123
Rytuba JJ, McKee EH (1984) Peralkaline ash flow tuffs and calderas of the McDermitt volcanic field, southeast Oregon and north central Nevada. J Geophys Res 89:8616–8628
Sakuyama M (1979) Evidence of magma mixing: petrological study of Shirouma-Oike calc-alkaline andesite volcano. Japan J Volcanol Geotherm Res 5:197–208
Sakuyama M (1981) Petrological study of the Myoko and Kurohime volcanoes, Japan: crystallization sequence and evidence for magma mixing. J Petrol 22:553–583
Schnetzler CC, Philpotts FA (1970) Partition coefficients of rare-earth elements between igneous matrix material and rock-forming mineral phenocrysts-II. Geochim Cosmochim Acta 34:331–340
Seifert F, Schreyer W (1965) Synthesis of a new mica, $KMg_{2.5}[Si_4O_{10}](OH)_2$. Amer Mineral 50:1114–1118
Shimizu N, Roex AP (1986) The chemical zoning of augite phenocrysts in alkaline basalts from Gough Island, South Atlantic. J Volcanol Geotherm Res 29:159–188
Sparks RSJ, Marshall LA (1986) Thermal and mechanical constraints on mixing between mafic and silicic magmas. J Volcanol Geotherm Res 29:99–124
Steven TA (1975) Middle Tertiary volcanic field in the southern Rocky Mountains. Geol Soc Amer Mem 144:75–94
Stormer JC Jr, Nichols J (1978) XLFRAC: a program for the interactive testing of magmatic differentiation models. Comput Geosci 4:143–159
Taylor RP, Strong DF, Fryer BJ (1981) Volatile control of contrasting trace element distributions in peralkaline granite and volcanic rocks. Contrib Mineral Petrol 77:267–271
Taylor SR (1964) The abundance of chemical elements in the continental crust – a new table. Geochim Cosmochim Acta 28:1273–1285
Thompson RA, Johnson CM (1987) Oligocene basaltic volcanism of the San Luis Hills, northern Rio Grande rift, Colorado. Geol Soc Amer Abs Prog 19:868
Thompson RA, Dungan MA, Lipman PW (1986) Multiple differentiation processes in early-rift calc-alkaline volcanics, northern Rio Grande rift, New Mexico. J Geophys Res 91:6046–6058
Watson EB (1979) Zircon saturation in felsic liquids: experimental results and applications to trace element geochemistry. Contrib Mineral Petrol 70:407–419
Weaver SD (1976) The Quaternary caldera volcano Emuruangogolak, Kenya rift, and the petrology of a bimodal ferrobasalt-pantelleritic trachyte association. Bull Volcanol 40:209–230
Wolff JA, Storey M (1984) Zoning in highly alkaline magma bodies. Geol Magm 121:563–575

Received October 10, 1987 / Accepted May 31, 1988

Editorial responsibility: T. Grove